How CD4+ T-cell help shapes functional and dysfunctional CD8+ T-cell differentiation

Busselaar, J.L.C.

Chapter 4

Stem-like PD-1$^+$TCF-1$^+$ CD8$^+$ T cells result from helpless priming and rely on CD4$^+$ T-cell help to complete their cytotoxic effector differentiation

Julia Busselaar[1]*, Douwe M. T. Bosma[1]*, Mo D. Staal[1], Xin Lei[1], Yanling Xiao[1] and Jannie Borst[1]

[1]Department of Immunology and Oncode Institute, Leiden University Medical Center, Leiden, The Netherlands
*Shared first authors

The Journal of Immunotherapy of Cancer 2026; 14(4): e014041
DOI: 10.1136/jitc-2025-014041

Abstract

Antigen-specific CD8$^+$ T cells can be in a stem-like PD-1$^+$TCF-1$^+$ differentiation state that progresses into terminal exhaustion in cancer and chronic infection. These stem-like cells are important, since they are the responders to PD-1 targeted immunotherapy and a potential resource for anti-tumor immunity. We use a mouse vaccination model to delineate by spectral flow cytometry and single cell RNA sequencing the effects of CD4$^+$ T-cell help during priming on the differentiation fate of stem-like CD8$^+$ T cells. We use bioinformatic analysis to extrapolate our data to mouse models of cancer and chronic infection. We next explore CD8$^+$ T-cell differentiation states and delivery of CD4$^+$ T-cell help in the immunogenic MC38 tumor model. Upon vaccination in absence of help signals, stem-like CD8$^+$ T cells do not further differentiate and accumulate in the draining lymph node. When help signals are delivered, stem-like CD8$^+$ T cells proliferate and differentiate into circulating cytotoxic effector cells. Stem-like CD8$^+$ T cells raised by vaccination in presence or absence of CD4$^+$ T-cell help have an identical transcriptome, which they share with stem-like CD8$^+$ T cells defined in mouse models of cancer and chronic infection. The immunogenic MC38 tumor harbors endogenous helper epitopes, but primes stem-like CD8$^+$ T cells rather than helped cytotoxic effectors. Therapeutic vaccination with endogenous helper epitopes does not improve MC38 tumor control. Intra-tumoral expression of strong, exogenous helper epitopes as present in our vaccine improves tumor control, but does not efficiently convert stem-like tumor-specific CD8$^+$ T cells into helped cytotoxic effectors. Our data argue that stem-like CD8$^+$ T cells are helpless cells that lie at the bifurcation point of CD8$^+$ T-cell effector- and exhaustion trajectories. Even though the immunogenic MC38 tumor expresses helper epitopes, it primarily raises stem-like CD8$^+$ T cells, indicating that help delivery is impaired in this tumor context. Promoting the efficient delivery of help signals to stem-like tumor-specific CD8$^+$ T cells to drive their expansion and differentiation into cytotoxic effectors is therefore an important therapeutic challenge in cancer and other conditions that lead to T-cell exhaustion.

Introduction

In a CTL response that results in antigen clearance, differentiation of newly activated CD8+ T cells is described as a trajectory ranging from the naïve state, via central memory (T_{CM}) and effector memory (T_{EM}) precursor states to a terminally differentiated effector CTL state[1,2]. When antigen persists, such as in chronic infection and cancer, CD8+ T cells differentiate along an exhaustion trajectory, characterized by poor cytolytic function and expression of coinhibitory receptors, including PD-1[3]. "Stem-like", "(pre)dysfunctional" or "progenitor exhausted (Tpex)" cells lie early in this trajectory, marked by co-expression of transcription factor TCF-1 and PD-1, next to CXCR5 and SLAMF6[4,5]. Stem-like CD8+ T cells are of interest, since they respond to PD-1-targeted immune checkpoint blockade (ICB) to generate functional CTLs in mouse models and are associated with ICB response in human cancer[6]. Recent meta-analyses of mRNA- and TCR sequencing (seq) datasets have mapped stem-like CD8+ T cells at the branchpoint of differentiation trajectories towards either the functional CTL effector state or the terminally exhausted state[7,8]. Stem-like cells are formed during both acute and chronic infection, consistent with the concept that they can differentiate into either cell state[9,10]. To improve immunotherapy strategies, it is crucial to know how stem-like CD8+ T cells can be instructed to become competent CTL effectors[3,6].

We here test the hypothesis that stem-like CD8+ T cells lie on a potentially productive CTL effector differentiation trajectory that can be completed when CD4+ T-cell help signals are provided[11]. During priming in lymph nodes (LNs), CD4+ T cells can deliver "help" for the CTL response, via conventional (c) dendritic cells (DCs). CD4+ and CD8+ T cells are initially activated separately, in distinct regions of the LN by migratory cDCs. When conditions permit, activated CD4+ and CD8+ T cells are subsequently guided by chemokine cues to recognize their respective antigens on the same cDC1[12]. In this cellular scenario, help for the CTL response is delivered[13,14]. The CD4+ T cell "licenses" the cDC1 to relay help signals to CD8+ T cells, by endowing it with optimal antigen cross-presentation and cross-priming capacity, which is facilitated by costimulatory molecules such as CD70, as well as specific cytokines and chemokines[15–19]. Help signals instruct the CD8+ T cell to acquire optimal CTL effector[20] and effector memory[21] differentiation programs, hallmarked in the primary effector phase by downregulation of inhibitory receptors and increased cytotoxic, migratory and invasive capacities, which are pivotal for tumor control[20]. Conversely, "helpless" CTLs, i.e. CD8+ T cells primed in absence of CD4+ T-cell help, have all the typical hallmarks of CTL dysfunction[11,20,22].

Inflammatory signals, in particular IFN-I, make a key contribution to cDC1 licensing[17,23]. IFN-I acts in synergy with CD4+ T-cell mediated CD40 signaling to induce the gene expression program of the licensed cDC1[19]. Innate signaling by IFN-I as elicited e.g. by virus infections often seems to compensate for CD4+ T-cell help in the primary CTL response, but help is generally required for generation of adequate CD8+ T-cell memory[14,24]. This conundrum has recently been solved by the finding that CD4+ T-cell help does improve the primary CTL response to virus infection, but

this contribution is obscured when conventional and regulatory CD4$^+$ T cells are co-depleted to eliminate "help"[25]. In chronic LCMV infection, CD4$^+$ T-cell depletion promotes CD8$^+$ T-cell exhaustion[26] and reduces formation of virus-controlling effector CTLs, but not stem-like cells[27,28]. These data suggest that lack of help promotes CD8$^+$ T-cell differentiation along the exhaustion trajectory when antigen persists.

Based on these concepts, we have postulated that stem-like cells as found in chronic infection and cancer may result from helpless priming[11]. Here, we tested the impact of CD4$^+$ T-cell help on formation and fate of stem-like CD8$^+$ T cells in a well-defined vaccination model, in which we previously determined at the molecular level how CD4$^+$ T-cell help improves function of CD8$^+$ T-cell effector and effector memory cells[20,21]. We demonstrate that PD-1$^+$TCF-1$^+$ stem-like CD8$^+$ T cells lie on a potentially productive effector differentiation trajectory that is completed in non-tumor-bearing mice when help signals are delivered by vaccination. However, in an immunogenic MC38 tumor context, help delivery and CTL effector differentiation are impaired, both before and after therapeutic vaccination, even when a CD4$^+$ T-cell response to tumor-intrinsic epitopes takes place.

Results

Stem-like CD8$^+$ T cells predominate after priming in absence of CD4$^+$ T-cell help

To compare CD8$^+$ T-cell responses in presence or absence of CD4$^+$ T-cell help, we use two DNA vaccines: one encoding the immunodominant E7$_{48\text{-}57}$ peptide of human papilloma virus (HPV) that only primes E7-specific CD8$^+$ T cells (No Help) and one additionally encoding HPV-unrelated MHC-II restricted helper epitopes P30/PADRE that also primes CD4$^+$ T cells[29,30] (Help) (Figure 1A). The plasmid DNA is "tattooed" into the epidermis, resulting in antigen expression in keratinocytes and efficient T-cell priming by migratory cDCs in the skin-draining inguinal LN[29,31]. Mice are vaccinated at day 0, 3 and 6, after which the antigen-specific CD8$^+$ T-cell response is followed by H-2D^b/E7$_{48\text{-}57}$ (E7) tetramer staining (Supplementary Figure 1A-C). In this transparent model, antigen is only transiently present during priming[31,32] and the impact of CD4$^+$ T cells during priming on long-term CD8$^+$ T-cell fate is tested by their vaccine-based engagement in the response[29,30].

As previously shown[20,29], the E7-specific CD8$^+$ T-cell response to No Help vaccination was lower and of shorter duration than the response to Help vaccination (Figure 1B) and at day 10, the frequency of E7-specific CD8$^+$ T cells was significantly lower in the No Help setting than in the Help setting in blood and spleen (Figure 1C). Moreover, in the No Help setting PD-1, TCF-1 and SLAMF6 that identify the stem-like state[6,28,33] were expressed at higher levels on E7-specific CD8$^+$ T cells in the dLN, which is the priming site (Figure 1D).

An extensive antibody panel was used to distinguish E7-specific CD8+ T-cell differentiation states[2,34] after Help or No Help vaccination in blood, spleen, dLN and ndLN. At day 10 after vaccination, clustering analysis and dimension reduction on cumulative E7-tetramer+ CD8+ T cells resulted in 10 clusters (Figure 1E), which were differentially distributed between vaccination settings (Figure 1F, Supplementary Figure 1D) and between organs (Supplementary Figure 1D, E). Cluster 1 cells were higher in frequency among tetramer+ CD8+ T cells (Figure 1G) and total CD8+ T cells (Supplementary Figure 1F) after Help than after No Help vaccination and were mostly found in the circulation, i.e. in blood and spleen**.** Cluster 1 cells were characterized by low expression of CD62L and TCF-1 and high expression of KLRG1 and CX3CR1 (Figure 1H), consistent with a terminally differentiated, short-lived effector CTL state[35,36]. In LNs, Cluster 6 cells were higher in frequency among tetramer+ CD8+ T cells (Figure 1I) and total CD8+ T cells (Supplementary Figure 1F) in the No Help setting than in the Help setting and characterized by high levels of TCF-1, SLAMF6 and PD-1 and low levels of KLRG1 and CX3CR1 (Figure 1H), indicating the stem-like phenotype[6,28,33]. Consistent with vaccination rather than chronic antigen exposure, exhausted CD8+ T cells with a PD-1^{high}TIM3+TCF-1- phenotype[4] were not observed (Supplementary Figure 1G). These results indicate that in presence of CD4+ T-cell help during priming, CD8+ T cells can terminally differentiate into CTL effector cells that distribute systemically through blood and spleen. In absence of CD4+ T-cell help, primed CD8+ T cells accumulate in the PD-1+TCF-1+ stem-like state in LNs.

CD4+ T-cell help shifts the CD8+ T-cell differentiation spectrum towards the effector state

To analyze the effects of CD4+ T-cell help on the CTL differentiation spectrum, we mapped the antigen-specific CD8+ T-cell clusters as defined in Figure 1 using the Wanderlust algorithm that aligns cells to a unified trajectory based on overlap in marker expression[37]. This procedure generated a CTL differentiation trajectory ranging from the naïve state (CD44-CD62L+) to the short-lived effector state (KLRG1+CX3CR1+) (Figure 2A). After Help vaccination, CD8+ T cells in dLN, spleen and blood had a higher mean trajectory score than after No Help vaccination (Figure 2B), indicating that on average, CD4+ T-cell help shifts the differentiation state of CD8+ T cells towards completion of the trajectory.

To visualize the calculated trajectory along the progressive differentiation path as described in literature[1,2,34], we mapped protein expression of differentiation markers of naïve (CD44-CD62L+TCF-1+), T stem cell memory (T_{SCM})/T_{CM} precursor (CD44+CD62L+TCF-1+), stem-like (PD-1+TCF-1+SLAMF6+), T_{EM} precursor (CD44+CD62L-) and effector (KLRG1+CX3CR1+) cell states against the trajectory (Figure 2C, Supplementary Figure 2). PD-1 and SLAMF6 were upregulated halfway through the trajectory, in CD8+ T cells that retained TCF-1 expression, corroborating that PD-1+TCF-1+SLAMF6+ stem-like cells are in an early differentiation state. These cells highly expressed proliferation marker Ki67, in agreement with literature data[33,38,39]. Further differentiation along the trajectory towards effector cells was associated with downregulation of PD-1, TCF-1 and SLAMF6 and upregulation of CX3CR1 and KLRG1 (Figure 2C).

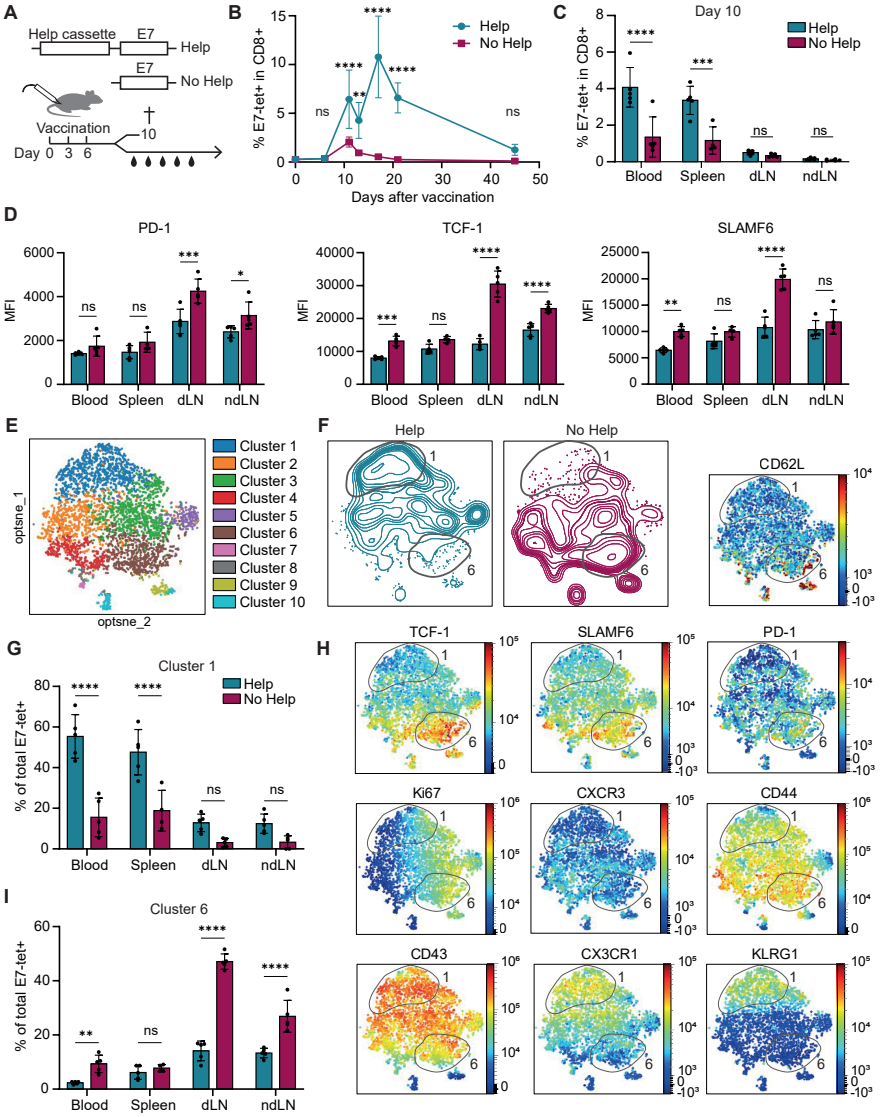

Figure 1. Stem-like CD8⁺ T cells predominate after priming in absence of CD4⁺ T-cell help. (A) Vaccination model. (B-I) The response of E7-tetramer⁺ CD8⁺ T cells to vaccination was analyzed by flow cytometry with antibodies to differentiation markers. (B, C) Percentage of E7-tetramer⁺ CD8⁺ T cells in indicated organs at the indicated days after the first vaccination. (D) Median Fluorescence Intensity (MFI) of indicated markers on E7-tetramer⁺ CD8⁺ T cells at day 10. (E, F) Opt-SNE visualization of E7-tetramer⁺ CD8⁺ T cells at day 10. FlowSom clustering of cells from all experimental settings (E) and distribution of cells from the two vaccination settings (F). Clusters 1 and 6 are encircled. (G, I) Frequencies of E7-tetramer⁺ CD8⁺ T cells in Cluster 1 (G) and Cluster 6 (I) per organ. (H) Differentiation marker expression on cumulative E7-tetramer⁺ CD8⁺ T cells from all experimental settings visualized by opt-SNE. Data are from 1 experiment, representative of at least 2 independent experiments with n=5 mice per group. Error bars indicate SD. Statistical significance was calculated by two-way ANOVA and Sidak's multiple comparisons test. ns, not significant, *P < 0.05, **P <0.005, ***P < 0.001 and ****P < 0.0001. See also Supplementary Figure 1.

Next, we plotted antigen-specific CD8+ T cells, harvested from blood, spleen and LNs after Help or No Help vaccination, against this differentiation spectrum based on their trajectory score (Figure 2D). Blood and spleen harbored cells with a high trajectory score of 0.8-1.0 (Figure 2D), corresponding to a KLRG1+CX3CR1+ phenotype (Figure 2C) after Help vaccination, while this population was much smaller after No Help vaccination. In LNs, cells had a lower trajectory score ranging from 0.3 to 0.8 (Figure 2B, D), predominated by the PD-1+TCF-1+SLAMF6+ phenotype (Figure 2C), both after Help and No Help vaccination. However, after Help vaccination, the LN cells had differentiated further than after No Help vaccination (Figure 2B, D).

We conclude that antigen-primed CD8+ T cells can differentiate into CD44+CD62L+ T_{CM} precursor and PD-1+TCF-1+SLAMF6+ stem-like populations irrespective of CD4+ T-cell help, but require CD4+ T-cell help to become CD44+CD62L- T_{EM} precursor and KLRG1+CX3CR1+ short-lived CTL effector cells.

Stem-like CD8+ T cells turn into effector cells upon receiving CD4+ T-cell help

If stem-like CD8+ T cells are indeed incompletely differentiated, one would expect them to arise earlier after priming than help-dependent effector CTLs. To test this assumption, we vaccinated mice under Help or No Help conditions and analyzed antigen-specific CD8+ T cells in the dLN at multiple successive days after the first vaccination (Figure 3A). After Help vaccination, E7-specific CD8+ T cells strongly increased in number from day 6 onwards, while after No Help vaccination the response was lower and more belated (Figure 3B). To exclude background tetramer staining of naïve CD8+ T cells, especially at early time points, we only included clusters that increased in size after vaccination (Supplementary Figure 3). Clustering and dimension reduction of cumulative responding CD8+ T cells indicated distinct phenotypes in Help and No Help settings, as expected (Figure 3C). We dissected responder CD8+ T cells into stem-like (TCF-1+SLAMF6+) and effector (GZMB+) subsets (Figure 3D, E) and analyzed the generation of these two populations over time. After Help vaccination, the stem-like population initially predominated, but from day 6 onwards it decreased, while the effector population increased (Figure 3F). After No Help vaccination, in contrast, the stem-like population steadily increased to form the majority of the E7-specific CD8+ T-cell pool in the dLN, while the effector cell population remained small (Figure 3G). These results indicate that stem-like CD8+ T cells are generated early after priming, in both presence and absence of CD4+ T-cell help. However, only in presence of CD4+ T-cell help, these cells in time further differentiate into effector CTLs.

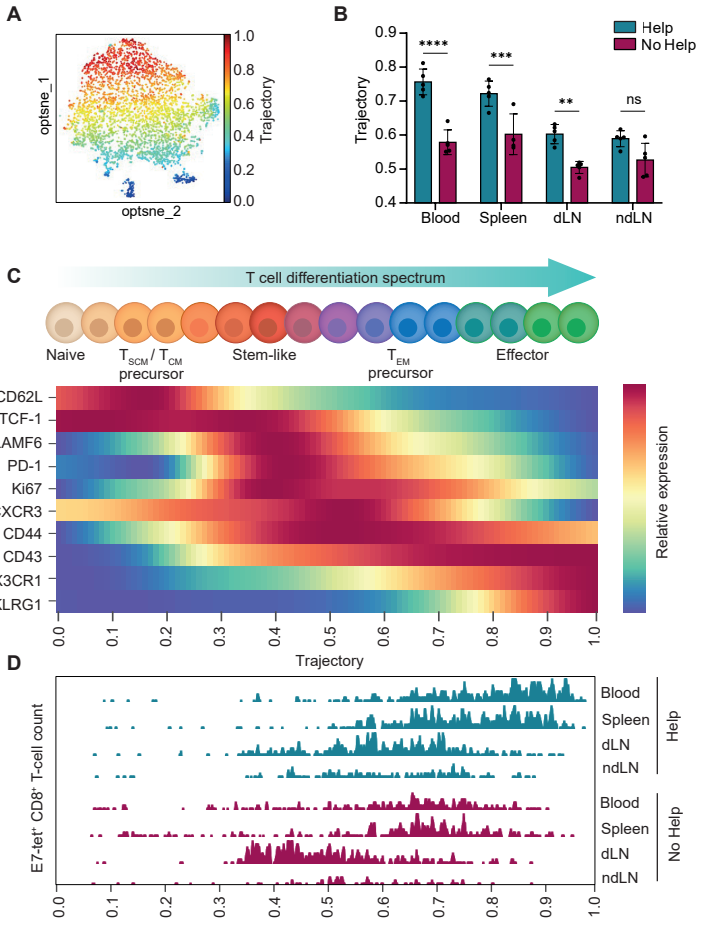

Figure 2. CD4⁺ T-cell help shifts the CD8⁺ T-cell differentiation spectrum towards the effector state. Mice were vaccinated and analyzed at day 10 as outlined in Figure 1 (same experiment). (A) Wanderlust trajectory shown as color gradient within opt-SNE visualization of all E7-tetramer⁺ CD8⁺ T cells from all organs. (B) Mean trajectory score of E7-tetramer⁺ CD8⁺ T cells from indicated organs. (C) CD8⁺ T-cell differentiation states as defined in literature were mapped to the trajectory axis based on marker expression. Heat map shows relative expression level of differentiation markers on E7-tetramer⁺ CD8⁺ T cells, as determined per marker on lowest and highest level observed. (D) Distribution of E7-tetramer⁺ CD8⁺ T cells from indicated organs after Help or No Help vaccination along the differentiation trajectory. Data are from 1 experiment, representative of 2 independent experiments with n=5 mice per group. Error bars indicate SD. Statistical significance was calculated by two-way ANOVA and Sidak's multiple comparisons test. ns, not significant, *P < 0.05, **P< 0.005, ***P < 0.001 and ****P <0.0001. See also Supplementary Figure 2.

It is an important question whether stem-like CD8+ T cells primed in absence of CD4+ T-cell help can still complete their effector differentiation when help signals are delivered after priming. To test this, we used adoptive transfer with OT-I T cells that express a transgenic TCR recognizing the ovalbumin $(OVA)_{257/264}$/H-2K^b complex (Figure 3H). CD45.2+ mice received 10^5 naïve CD45.1+ OT-I cells and OVA-No Help vaccine encoding the $OVA_{257/264}$ epitope. At day 10, CD45.1+CD44+SLAMF6+ stem-like OT-I cells were flow sorted from pooled dLNs (Supplementary Figure 4A) and transferred at 10^4 per mouse into CD45.2+ secondary recipient mice. The next day, so still in the effector phase of the response, these mice received either control OVA-No Help or test OVA-Help vaccine with the same helper epitopes as in the E7 Help vaccine. The vaccine encoded both helper and CTL epitopes to enable communication between CD4+ T cells and CD8+ T cells at the cDC1 interface[13,14]. Transferred stem-like OT-I T cells clonally expanded upon OVA-Help vaccination, but not upon OVA-No Help vaccination (Figure 3I, J, Supplementary Figure 4B). After Help vaccination, a proportion of the transferred OT-I T cells gained the help-dependent KLRG1+CX3CR1+ effector phenotype as compared to the OT-I population at transfer (Figure 3K, L, Supplementary Figure 4C), primarily in blood and spleen (Figure 3M). Together, these results demonstrate that helpless stem-like CD8+ T cells can still respond to help signals after initial priming by expansion, CTL effector differentiation and systemic dissemination.

Combined scRNAseq and TCRseq analyses support that stem-like CD8+ T cells differentiate into CTL effectors upon CD4+ T-cell help delivery

To test directly whether addition of CD4+ T-cell help signals leads to the transition of stem-like CD8+ T cells into effector CTLs, we performed single cell RNA sequencing (scRNAseq) and TCR sequencing (TCRseq). For this purpose, mice received E7-Help or E7-No Help vaccine and at day 5 or day 10, activated CD3+CD44+CD62L- T cells were sorted by flow cytometry from both dLN and ndLN (Supplementary Figure 5). This resulted in eight samples that were labeled with distinct hashtag oligonucleotides (HTO)-conjugated antibodies before performing scRNAseq and TCRseq on pooled cells (Supplementary Figure 6A, B). For analysis, we used CD8+ T cells isolated from dLNs at days 5 and 10 after Help vaccination and at day 10 after No Help vaccination, since these HTO groups yielded sufficient CD8+ T-cell numbers as identified based on *Cd8a* and *Cd8b1* expression (Supplementary Figure 6C, D).

Whole transcriptome-based clustering of 3051 CD8+ T cells pooled from these three experimental conditions identified seven distinct cell states (Figure 4A), based on specific transcripts (Supplementary Table 1). Naive cells (Cluster 0) and T_{CM} cells (Cluster 1) were identified by co-expression of *Sell* (encoding CD62L), *Il7r* and *Ly6c2*, while naive cells expressed higher levels of *Lef1* and *Ccr7* and T_{CM} cells expressed *Eomes* (Figure 4B). Stem-like cells (Cluster 2) were identified by high expression of *Tcf7* (encoding TCF-1), *Id3* and *Slamf6,* next to *Sell*, *Lef1* and *Ccr7*. CTL effector cells (Cluster 3) were characterized by expression of *Gzmb*, *Gzmk*, *Id2* and *Tbx21* (encoding T-bet), and expressed various killer lectin receptor (KLR) genes such as *Klrc1* and *Klrk1* and proliferation-associated genes including *Mki67, Tk1 and Kif11*. Some smaller clusters were characterized by expression of KLRs (Cluster 4), protein/RNA biosynthesis genes (Cluster 5), and IFN-I responsive genes (Cluster 6).

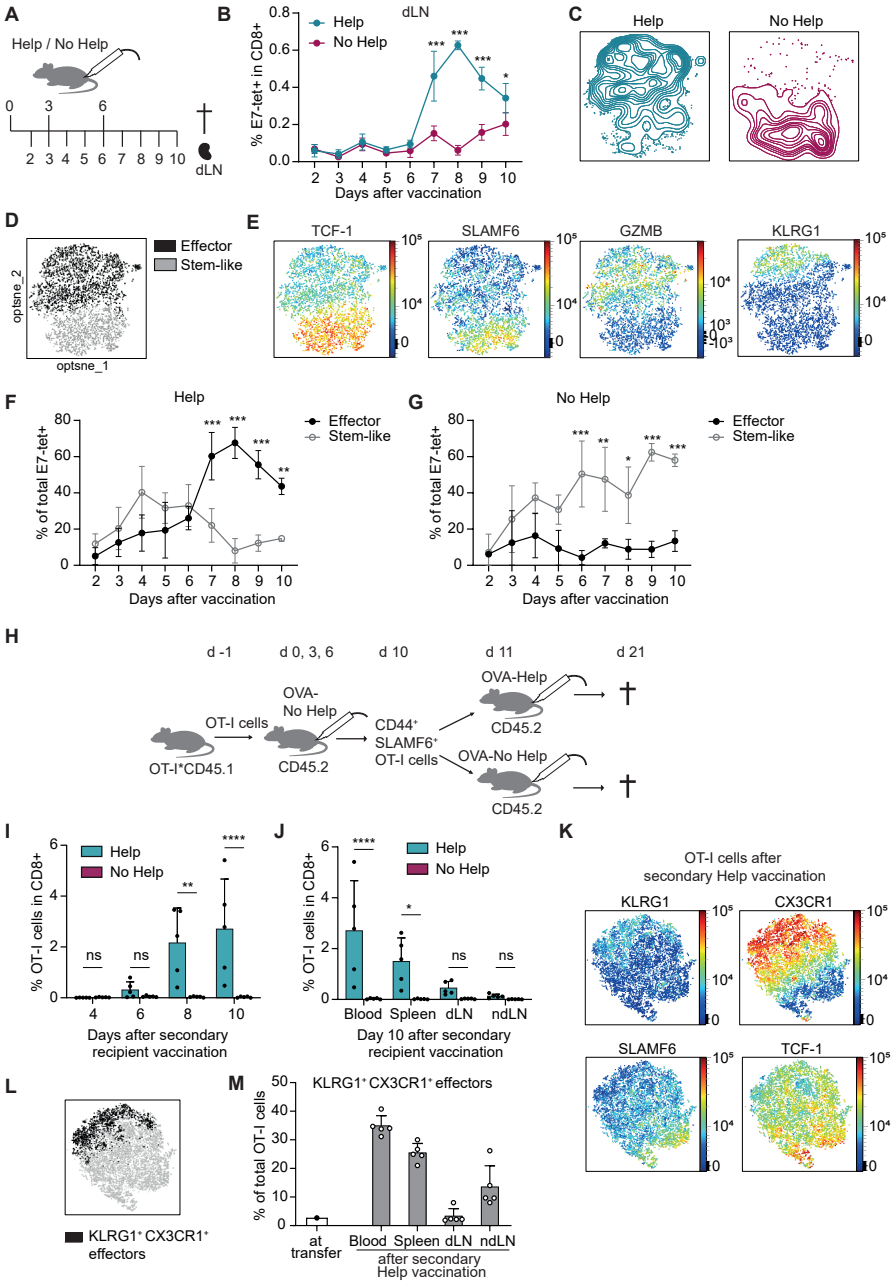

Figure 3. Formation of effector but not stem-like CD8⁺ T cells relies on CD4⁺ T-cell help. (A) Experimental setup for panels B-G. At different time points after Help or No Help vaccination, E7-specific CD8⁺ T cells in the dLN were analyzed by flow cytometry with the differentiation marker panel. (B) Frequency of E7-tetramer⁺ CD8⁺ T cells in dLNs. (C-E) Opt-SNE visualization of all responding E7-tetramer⁺ CD8⁺ T cells (see Supplementary Figure 3) in the dLN at all time points. (C) Distribution of responder CD8⁺ T cells from Help versus No

Help vaccination settings. (D) Visualization of stem-like (TCF-1+SLAMF6+) and effector (GZMB+) clusters. (E) Visualization of differentiation marker expression. (F, G) Frequency of stem-like and effector populations as defined in C-E within total responder E7-tetramer+ CD8+ T cells. (H) Experimental setup for panels I-M. (I, J) Frequency of OT-I (CD45.1+OVA-tetramer+ CD8+) T cells in secondary recipients, as measured in indicated organs at indicated time points. (K, L) Opt-SNE visualization of OT-I T cells in secondary recipients at day 10 after Help vaccination. (K) Expression of differentiation markers across opt-SNE. (L) Visualization of the KLRG1+CX3CR1+ effector population. (M) Frequency of KLRG1+CX3CR1+ effector cells (as defined in L) within the OT-I T cell population in indicated organs after secondary Help vaccination, and frequency of KLRG1+CX3CR1+ cells in the pooled OT-I population at transfer (as identified by manual gating). Data from B-G and I-M are each from 1 experiment, representative of 2 independent experiments with n=3-5 mice per group. Error bars indicate SD. Statistical significance was calculated by two-way ANOVA and Sidak's multiple comparisons test. ns, not significant, *P < 0.05, **P < 0.005, ***P < 0.001 and ****P < 0.0001. See also Supplementary Figure 3 and 4.

Clonal expansion within each CD8+ T-cell cluster was assessed by TCRseq analysis. Expanded clones, defined as TCR clonotypes containing ≥ 2 cells, were quantified for each cluster (Supplementary Figure 7A). This analysis revealed that, in agreement with proliferation marker expression, the effector population (Cluster 3) displayed much higher clonal expansion than any of the other clusters, both by number of distinct expanded clones and number of individual cells per clonotype (Figure 4C, Supplementary Figure 7B). The great majority of expanded TCR clonotypes were exclusively present in Cluster 3, while some were shared between Clusters 2 and 3 (Supplementary Figure 7C).

Pseudotime analysis based on calculating gene expression changes associated with dynamic biological processes[40] identified the stem-like population (Cluster 2) as an intermediate state between the naive (Cluster 0) and effector (Cluster 3) CD8+ T-cell differentiation states (Figure 4D, E). Importantly, effector CD8+ T cells lying at the end of the differentiation trajectory (Cluster 3) were abundantly present in the day 10 Help condition but mostly lacking in the day 10 No Help condition (Figure 4D). Under Help conditions, Cluster 3 effector cells increased in frequency from day 5 tot day 10 after vaccination (Figure 4F). Accordingly, CD8+ T cells from the day 10 Help condition showed a higher median pseudotime score as compared to cells from the other two experimental conditions (Figure 4E). They also showed a higher number of distinct expanded clones (Supplementary Figure 7D, E), and a higher number of cells per TCR clonotype (Supplementary Figure 7F), in agreement with clonal expansion being most prominent in Cluster 3 (Figure 4C). Stem-like CD8+ T cells (Cluster 2) were generated both under No Help and Help conditions (Figure 4D, F) but predominated under No Help conditions at day 10 (Figure 4F). Importantly, Cluster 2 stem-like CD8+ T cells from Help and No Help conditions had indiscernible transcriptomes at day 10 (Figure 4G). Differential gene expression analysis between Cluster 2 and 3 followed by Ingenuity Pathway Analysis (IPA) showed that functional qualities of helped CD8+ T cells, such as cytotoxicity, cell migration and proliferation, were acquired upon differentiation from the stem-like to the effector state (Supplementary Figure 8A-D, Supplementary Table 2). These findings agree with our earlier study in the same vaccination model, where we used bulk

RNAseq of primed CD8$^+$ T cells from the No Help and Help settings at day 10 in the spleen to define the CTL effector differentiation program installed as a result of CD4$^+$ T-cell help[20].

Taken together, the current results show at the single cell level that the differentiation spectrum of CD8$^+$ T cells primed in presence of CD4$^+$ T-cell help includes both stem-like and effector cells, with effector cells expanding and predominating in time. In absence of help, the same stem-like CD8$^+$ T cells are formed that do not further differentiate into effector cells.

Stem-like CD8$^+$ T cells that predominate after helpless priming transcriptionally resemble stem-like CD8$^+$ T cells in chronic infection and cancer

Next, we determined how the stem-like and helped effector CD8$^+$ T-cell states from our vaccination system relate to CD8$^+$ T-cell states found in infection and cancer. We used primary data from mouse acute (Armstrong) and chronic (clone 13, CD4$^+$ T-cell depleted) LCMV infection models generated by Pritykin *et al.*[7] (Figure 5A). This study showed that the TCF-1$^+$ progenitor/stem-like state of CD8$^+$ T cells is epigenetically and transcriptionally comparable in classical models of chronic infection and cancer in mice. This study[7] and others[8,10] also demonstrated that the stem-like CD8$^+$ T-cell state lies at the basis of trajectories towards either effector CD8$^+$ T cells, as found in acute infection, or terminally exhausted CD8$^+$ T cells, as found in chronic infection and cancer (Figure 5B). We used the top 200 signature genes of the TCF-1$^+$ progenitor state defined by Pritykin *et al.* (Supplementary Table 3) to determine similarity to Cluster 2 and Cluster 3 cells from our vaccination model by module scoring. The TCF-1$^+$ progenitor signature was clearly enriched in the stem-like Cluster 2 cells predominating after No Help vaccination (Figure 5C). Furthermore, the gene signature of effector CTLs responding to acute LCMV infection (Supplementary Table 3) was enriched in effector Cluster 3 cells that predominate after Help vaccination (Figure 5C).

We also investigated at the whole transcriptome level how stem-like CD8$^+$ T cells raised in our vaccination model compared to those raised by a tumor. For this purpose, we used a dataset derived from a genetically engineered mouse model of spontaneous lung cancer (KP-NINJA), wherein tumor cells express LCMV-derived foreign antigens[41] (Figure 5D). The authors showed that tumor-specific PD-1$^+$TCF-1$^+$ stem-like cells accumulated in the tumor-draining LN (TdLN), and that these largely shared their transcriptome with stem-like CD8$^+$ T cells from chronic LCMV infection. Module score analysis showed that the top-100 gene expression signature of TdLN-derived stem-like CD8$^+$ T cells (Supplementary Table 3) was highly enriched in the stem-like CD8$^+$ T cells raised in our vaccination model (Figure 5E, F). These data extrapolate our findings to a large array of data from commonly used mouse models of (chronic) infection and cancer, making it plausible that the TCF-1$^+$ progenitor from which both effector and exhausted cells can arise equals a primed CD8$^+$ T cell that has not (yet) received CD4$^+$ T-cell help to differentiate into an effector CTL.

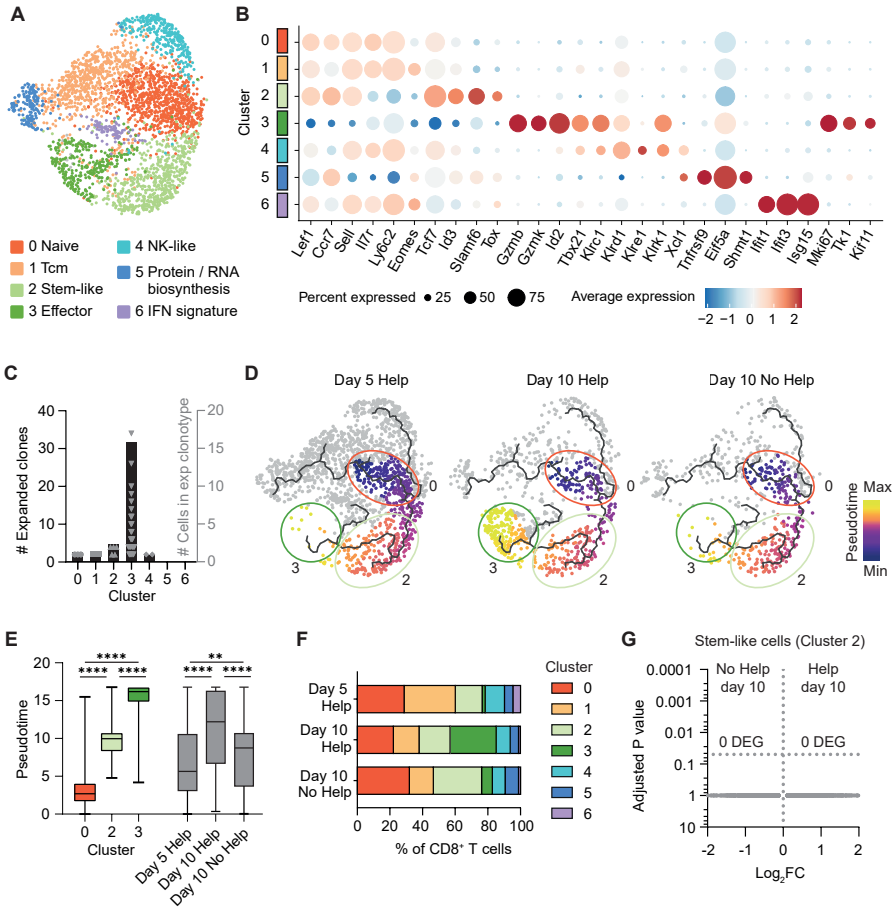

Figure 4. Combined scRNAseq and TCRseq support conversion of stem-like CD8⁺ T cells into CTL effectors upon CD4⁺ T-cell help delivery. Mice received Help or No Help vaccine (n=3 per group) and at days 5 and 10, activated CD3⁺CD44⁺CD62L⁻ T cells were flow cytometrically sorted from dLN and ndLN (See Supplementary Figure 5), labeled with different HTOs and subjected to 10x Genomics scRNAseq and coupled TCRseq (See Supplementary Figure 6). (A) UMAP projection and clustering of CD8⁺ T cells (defined in Supplementary Figure 6) from days 5 and 10 Help and day 10 No Help settings. (B) Level and frequency of CD8⁺ T-cell differentiation marker gene transcript expression, as identified by scRNAseq per CD8⁺ T-cell cluster. (C) TCR clonotype analysis. Number (#) of expanded CD8⁺ T-cell clonotypes (bars, left y-axis) as deduced from TCRseq per cluster, based on ≥ 2 cells with the same TCR, and number (#) of cells per expanded clonotype (symbols, right y-axis) per cluster (See also Supplementary Figure 7). (D) UMAPs showing pseudotime within the differentiation trajectory branch from naïve to effector gene expression profile, as based on scRNAseq data from the cumulative day 5 Help and day 10 Help and No Help conditions, plotted per indicated experimental condition. (E) Box plot showing pseudotime per cluster and per experimental condition. Statistical significance was calculated between clusters or between experimental conditions by two-way ANOVA and Sidak's multiple comparisons test. **P < 0.005 and ****P < 0.0001. (F) Distribution of CD8⁺ T cells over the different clusters (defined in A) per experimental condition. (G) Volcano plot showing 0 differentially expressed genes (DEG) between CD8⁺ cells within Cluster 2 from the day 10 Help versus No Help settings.

In an extension of the model of Pritykin *et al.*[7] and others[8,10], based on our current findings and review of the literature, we propose the following model: During CD8⁺ T-cell priming, stem-like cells are generated prior to delivery of CD4⁺ T-cell help signals. In case help signals are subsequently delivered, these stem-like cells are driven along a progressive differentiation trajectory into fully functional effector CTLs. When help signals are lacking and stem-like CD8⁺ T cells are exposed to chronic antigen stimulation under conditions as found in chronic infection and cancer, they follow the differentiation trajectory towards terminal exhaustion (Figure 5G).

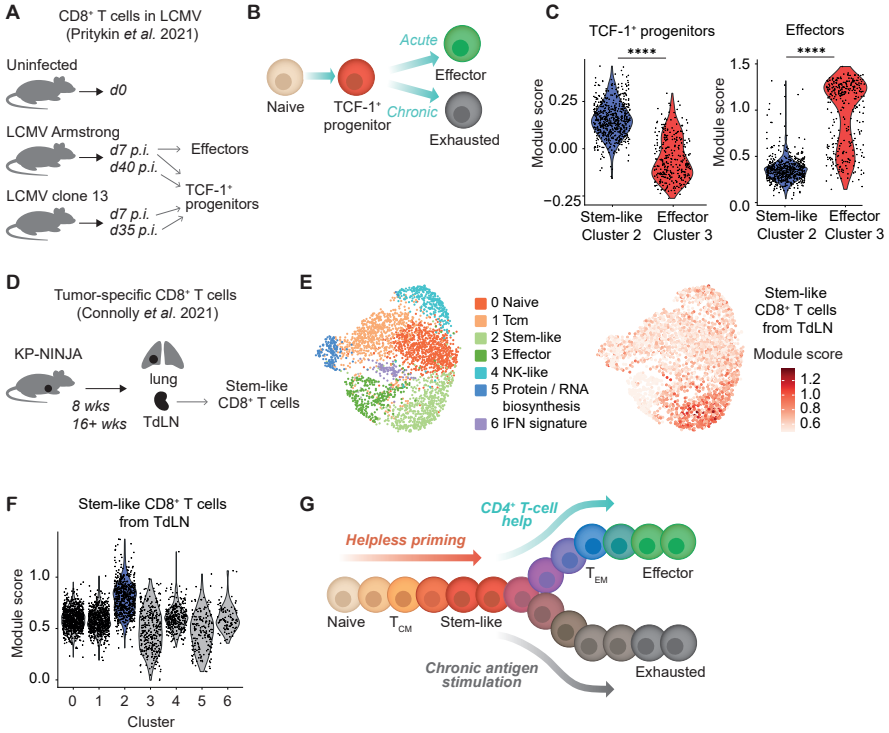

Figure 5. Stem-like CD8⁺ T cells that predominate after helpless priming transcriptionally resemble stem-like CD8⁺ T cells in chronic infection and cancer. (A) Outline of experimental conditions that generated the virus-specific CD8⁺ T cells analyzed by scRNAseq in Pritykin et al.[7]. (B) Differentiation model proposed by Pritykin et al.[7] and others[8,10]. (C) Violin plots showing module scores of the top 200 marker genes for CD8⁺ TCF-1⁺ progenitor cells (cluster 9, left panel) and effector cells (cluster 6, right panel) from Pritykin et al.[7] per CD8⁺ T cell in the stem-like Cluster 2 and helped effector Cluster 3 as defined in our vaccination model. Statistical significance was calculated by Mann-Whitney test. ****P < 0.0001. (D) Outline of experimental conditions that generated the tumor antigen-specific CD8⁺ T cells analyzed by scRNAseq in Connolly et al.[41]. (E, F) Module score of the top 100 marker genes for stem-like CD8⁺ T cells from TdLN (cluster 4, Connolly et al.[41]) per CD8⁺ T cell present in Cluster 2 and 3 in our vaccination model (Figure 4), as shown by UMAP (E) and violin plots (F). (G) Proposed model for CD8⁺ T-cell differentiation, wherein the PD-1⁺TCF-1⁺ stem-like state lies at the branchpoint of CD4⁺ T-cell help-dependent effector CTL differentiation and chronic antigen-driven CD8⁺ T-cell exhaustion in e.g. chronic infection and cancer.

The immunogenic MC38 tumor induces priming of neoantigen-specific stem-like, but not helped effector CD8+ T cells

We found earlier that therapeutic vaccination with the Help construct led to control of the HPV-E7+ TC-1 lung carcinoma, while No Help vaccination led to tumor outgrowth[29]. TC-1 tumor control after therapeutic Help vaccination was attributed to downregulation of inhibitory receptors, increased cytotoxicity and tumor invading capacities of CTLs as instructed by CD4+ T-cell help[20]. TC-1 is not spontaneously immunogenic and classifies as a lymphocyte-depleted, myeloid-rich tumor[42]. To investigate whether a spontaneously immunogenic tumor invites CD4+ T-cell help for the CTL response, we here used the T-cell infiltrated MC38 colon carcinoma model. MC38 tumor cells express defined MHC-I and MHC-II-restricted neoepitopes[43–45], which might enable spontaneous delivery of CD4+ T-cell help to the CTL response. To compare the differentiation states of CD8+ T cells raised by the MC38 tumor or by Help vaccination, we used a DNA vaccine encoding defined MC38-derived, MHC-I-restricted Rpl18 and Adpgk neoantigens[44] in conjunction with the Help cassette (Help-RA) (Figure 6A). Frequencies of Rpl18-tetramer+ CD8+ T cells spontaneously raised by MC38 tumors at day 15 were similar to those raised by Help vaccination at day 10 in blood, spleen and dLN. Rpl18-specific CD8+ T cells were also clearly detectable within the MC38 tumor (Figure 6B). We next compared neoantigen-specific CD8+ T-cell differentiation states in the MC38 and vaccination settings by flow cytometry (Supplementary Figure 9). In spleen and dLN of tumor-bearing mice, the frequency of PD-1+TCF-1+SLAMF6+ stem-like cells within the Rpl18-specific CD8+ T-cell pool was significantly higher than in vaccinated mice (Figure 6C). Conversely, in Help-RA vaccinated mice, the frequency of KLRG1+CX3CR1+ effector cells within the Rpl18-specific CD8+ T-cell pool was significantly higher than in tumor-bearing mice (Figure 6D). These results indicate that the MC38 tumor predominantly induces priming of stem-like CD8+ T cells and not help-dependent effector CTLs. Accordingly, the frequency of GZMB+ cells among Rpl18-specific CD8+ T cells and their GZMB protein levels were higher after vaccination than after MC38 tumor implantation (Figure 6E-G). Also, the frequencies of IFNγ+TNFα+ cells within total CD8+ T cells were higher in vaccinated mice than in tumor-bearing mice (Figure 6H, I). This reflected improved functional capacity rather than increased size of the responder population, since the frequency of antigen-specific CD8+ T cells in spleen was similar after vaccination or tumor inoculation (Supplementary Figure 9D).

Within the MC38 tumor, the great majority of Rpl18-specific CD8+ tumor infiltrating lymphocytes (TILs) expressed PD-1 and none of these cells had the KLRG1+CX3CR1+ helped effector phenotype (Supplementary Figure 9E-I), even though a fraction of them expressed GZMB (Supplementary Figure 9F). Also in the total CD8+ TIL population, GZMB+PD-1+ cells were found, while cells with a KLRG1+CX3CR1+ helped effector phenotype were lacking (Supplementary Figure 9H, I). Among Rpl18-specific TILs, the frequency of PD-1^{high}TIM3+TCF-1- exhausted cells[4] increased from day 7 to day 15 (Figure 6J), while the population of stem-like PD-1^{int}TCF-1+SLAMF6+ TILs decreased (Figure 6K), in line with the concept that stem-like cells become exhausted upon chronic antigen exposure in the TME. Accordingly, the frequency of Rpl18-specific GZMB+ TILs also decreased

upon tumor progression (Figure 6L). Among total CD8$^+$ TILs, a small proportion retained the capacity to produce IFNγ and TNFα after *in vitro* stimulation (Figure 6M).

We conclude that tumor-specific CD8$^+$ T cells primed by MC38 reach a stem-like differentiation state that develops into exhaustion in the TME, while they do not reach an effector differentiation state.

Delivery of CD4$^+$ T-cell help to CD8$^+$ T cells is impaired in the MC38 tumor context

We next tested whether therapeutic vaccination could deliver help to MC38-specific CD8$^+$ T cells. For this purpose, we used a 'neoHelp' cassette encoding MC38-derived MHC-II-restricted neoantigens Ddr2, Zmiz1 and Pcdh18[45] either alone (neoHelp), or in conjunction with MC38-derived MHC-I-restricted neoantigens Rpl18 and Adpgk (neoHelp-RA) (Figure 7A). Helper epitope vaccination did not change the frequency or the effector phenotype of Rpl18-specific CD8$^+$ T cells in blood over time compared to the empty vector (EV) control group (Figure 7B-D), nor did it improve survival of MC38 tumor-bearing mice (Figure 7E). Outside a tumor context, neoHelp-RA vaccination increased the frequency of Rpl18-specific CD8$^+$ T cells and their GZMB expression as compared to RA vaccination, but did not increase the formation of Rpl18-specific CD8$^+$ T cells with a KLRG1$^+$CX3CR1$^+$ effector phenotype (Supplementary Figure 10A-D). These data indicate that the neoantigen helper epitopes were functional, but not optimal in inducing CTL effector differentiation.

We therefore used another approach to introduce help for the CTL response by expressing in wild-type (wt) MC38 cells the strong helper epitopes P30 and PADRE as present in our standard vaccine Help cassette (Figure 7F). Next, we compared tumor-specific CD8$^+$ T-cell responses and tumor outgrowth in the MC38 wt and MC38-Help settings. The exogenous helper epitopes in the MC38-Help tumor were immunogenic as shown by the presence of a FOXP3$^-$CD44$^+$PADRE-tetramer$^+$ CD4$^+$ T-cell population in the spleen of mice bearing the MC38-Help tumor, but not the MC38 wt tumor (Figure 7G, Supplementary Figure 11A). Outgrowth of MC38-Help tumors was less efficient than that of MC38 wt tumors, resulting in lower tumor weight by day 15 and tumor clearance in 2 out of 10 mice (Figure 7H, I). The frequency of Rpl18-specific cells among CD8$^+$ TILs was higher in MC38-Help than in MC38 wt by day 15 (Figure 7J). However, the frequency of KLRG1$^+$CX3CR1$^+$ helped effector cells among Rpl18-tetramer$^+$ CD8$^+$ TILs was not different between the tumor settings (Figure 7K). Overall, the differentiation state of Rpl18-specific CD8$^+$ T cells in MC38 wt and MC38-Help tumors did not differ as assessed by the panel of differentiation markers, and most cells expressed PD-1 (Supplementary Figure 11B-E). The frequency of GZMB$^+$ cells among Rpl18-tetramer$^+$ CD8$^+$ TILs and total CD8$^+$ TILs was also not different between the two tumor settings (Figure 7L, Supplementary Figure 11F) and these cells were of a KLRG1$^-$CX3CR1$^-$PD-1$^+$ phenotype (Supplementary Figure 11G-I). CD8$^+$ TILs in both tumor settings had similar phenotypes, were largely PD-1$^+$ and cells with a KLRG1$^+$CX3CR1$^+$ helped effector phenotype were lacking. Likewise, the frequencies of CD8$^+$ TILs capable of producing IFNγ and TNFα upon *ex vivo* stimulation with Rpl18 and Adpgk neoantigen peptides did not differ (Supplementary Figure 11J).

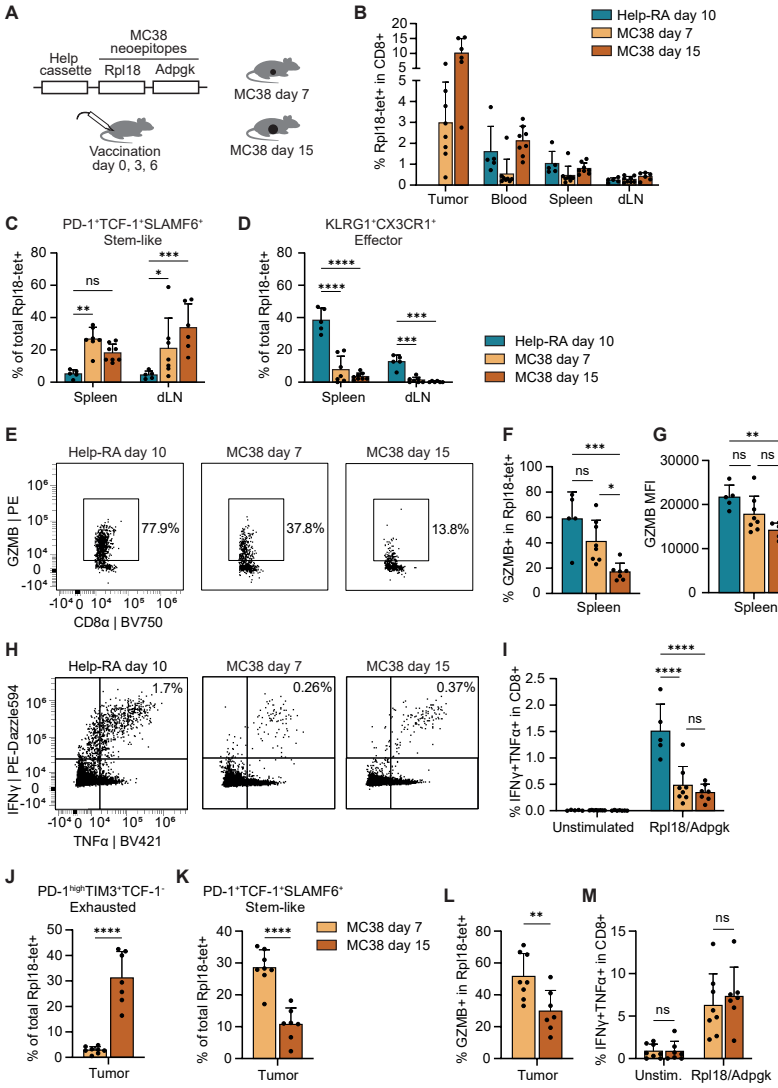

Figure 6. The MC38 tumor induces priming of neoantigen-specific stem-like, but not helped effector CD8⁺ T cells. (A) Experimental setup, mice were vaccinated or implanted with the MC38 tumor. (B) Frequency of Rpl18-tetramer⁺ CD8⁺ T cells in indicated tissues and the MC38 tumor. (C, D) Frequency of PD-1⁺TCF-1⁺ stem-like (C) and KLRG1⁺CX3CR1⁺ effector cells (D) within the Rpl18-specific CD8⁺ T-cell pool in the indicated organs. (E-G) Frequency of Granzyme-B (GZMB)⁺ cells within the Rpl18-specific CD8⁺ T cell population in spleen (E, F), and MFI of GZMB in this population (G). (H, I) Frequency of IFNγ⁺TNFα⁺ cells within the CD8⁺ T cell population from spleen after ex vivo stimulation with Rpl18 and Adpgk neoantigen peptides. (J, K) Frequency of PD-1^{hi}TIM3⁺TCF-1⁻ exhausted (J) and PD-1⁺TCF-1⁺ stem-like cells (K) within the CD8⁺ TIL pool on day 7 or 15 after tumor inoculation. (L) Frequency of GZMB⁺ cells within Rpl18-specific CD8⁺ TILs. (M) Frequency of IFNγ⁺TNFα⁺ cells within CD8⁺ TILs upon ex vivo restimulation with Rpl18 and Adpgk peptides. Data in A-D and E-M are from 2 separate experiments with n=5-8 mice per group. Error bars indicate SD. Statistical significance was calculated by two-way (B-D, I, M) or one-way (F, G) ANOVA and Sidak's multiple comparisons test, or unpaired t-test (J, K). ns, not significant, *P < 0.05, **P < 0.005, ***P < 0.001 and ****P < 0.0001. See also Supplementary Figure 9.

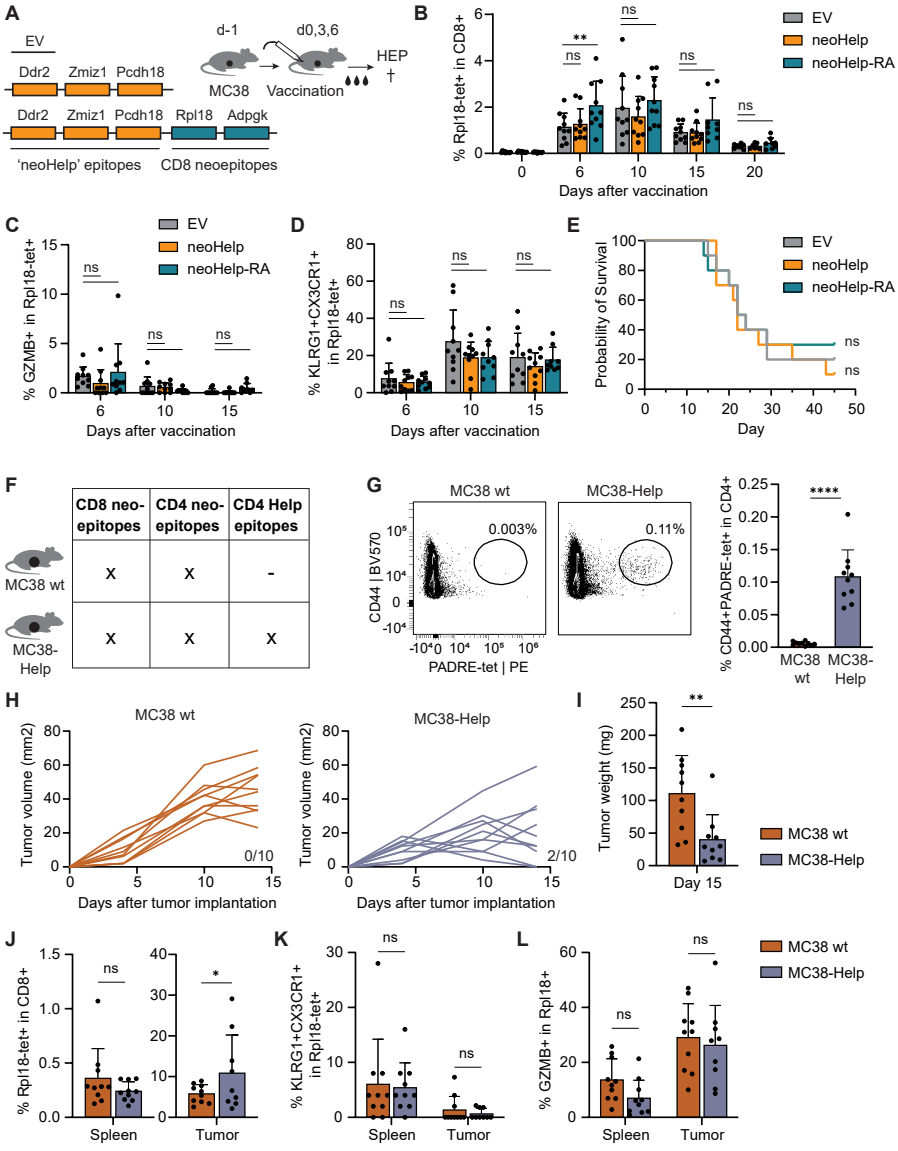

Figure 7. Delivery of CD4⁺ T-cell help to CD8⁺ T cells through vaccination or helper epitope expression is impaired in the MC38 tumor context. (A) Experimental outline. Mice were s.c. inoculated with 300.000 MC38 tumor cells on day -1, and vaccinated on day 0, 3, and 6 with DNA encoding empty vector (EV), neoHelp (MC38-derived MHC-II restricted neoepitopes mutated Ddr2, Zmiz1 and Pcdh13) or neoHelp-Rpl18-Adpgk (neoHelp-RA, containing both MC38-derived MHC-II and MHC-I restricted neoepitopes). Tumor outgrowth, survival and MC38-specific (Rpl18-tetramer⁺) CD8⁺ T-cell responses in blood were assessed over time. (B) Frequency of Rpl18-tetramer⁺ CD8⁺ T cells in blood at various timepoints. (C, D) Frequency of Granzyme-B (GZMB)⁺ cells (C) and KLRG1⁺CX3CR1⁺ effector cells (D) within the Rpl18-tetramer⁺ CD8⁺ T cell pool. (E) Survival plot. (F) MC38 tumor cells for which endogenous MHC-I and MHC-II restricted neoepitopes have been defined were transduced to stably express the Help cassette (P30/PADRE) as present in our vaccine, resulting in the MC38-Help tumor line. (G-L) Mice were

inoculated with 300.000 MC38 or MC38-Help cells (legend for all panels as indicated in Panels D and I) at day 0 and analyzed at day 15. (G) Frequency of CD44+PADRE-tetramer+ among CD4+ T cells in spleen. (H) Outgrowth of MC38 and MC38-Help tumors until day 15. Numbers of mice with complete tumor clearance are indicated. (I) Tumor weight at day 15. (J) Frequency of Rpl18-tetramer+ CD8+ T cells in spleen and tumor. (K) Frequency of KLRG1+CX3CR1+ effector cells within the Rpl18-specific CD8+ T-cell pool in the indicated organs. (L) Frequency of Granzyme-B (GZMB)+ cells within Rpl18-specific CD8+ T cells in spleen and tumor. Data in B-E are from 1 experiment with n=10 mice per group. Data in G-L are from 1 experiment representative of 2 independent experiments with n=10 mice per group. Error bars indicate SD. Statistical significance was calculated by two-way ANOVA and Sidak's multiple comparisons test (B-D, J-L), Mantel-Cox log-rank test (E) or unpaired t-test (G, I). In B-E, statistical significance was calculated in comparison to the EV group. ns, not significant, *P < 0.05, **P < 0.005, ***P < 0.001 and ****P < 0.0001. See also Supplementary Figure 11.

In conclusion, deliberate expression of strong helper epitopes in MC38 tumor cells raised tumor-specific CD4+ T cells and increased the frequency of tumor-specific CD8+ T cells. However, these CD8+ T cells lacked the helped effector phenotype, suggesting that CD4+ T-cell help was not efficiently delivered in this tumor context. Tumor control was moderately improved, which may have been due to the increase in tumor-specific CD8+ T cells resulting from help signals, but also to CD4+ T-cell help delivered to B cells or myeloid cells.

Discussion

By bulk RNAseq, we have shown that CD4+ T-cell help downregulates coinhibitory receptors on primed CD8+ T cells and strongly promotes their cytotoxic and migratory capacities[20]. Here, we define in the same model at the single cell level that CD4+ T-cell help promotes the differentiation of CD8+ T cells from the stem-like to the CTL effector state, which is accompanied by clonal expansion. Our results are in line with the linear model of CD8+ T-cell differentiation, which proposes a spectrum of CD8+ T cell states ranging from stem-like memory populations with low differentiation states to (short-lived) effector T cells with a terminal differentiation state[1,2,46,47]. Our data explain the increased functionality that we and others have described for helped CD8+ T cells[20–22] as a shift in this differentiation spectrum towards the effector state. The here determined nature of this shift also explains our earlier finding that CD4+ T-cell help increased the number and functionality of T_{EM} cells, but not of more stem-like T_{CM} cells[21].

Importantly, we did not exclusively raise effector CTLs upon Help vaccination, but cells ranging along the entire CD8+ T-cell differentiation spectrum, including stem-like cells. On phenotypic and transcriptomic level, stem-like cells from the Help and No Help vaccination settings were identical, suggesting that these cells have received the same signals during priming. We propose therefore that stem-like cells generated after Help vaccination also represent helpless cells, that have undergone the first step of priming but have not yet received CD4+ T-cell help. After Help vaccination, stem-like cells in the dLN turn into effector cells over time, in accordance with the idea that help is delivered in a second step of priming[14].

The progressive differentiation model proposes that CD8$^+$ T-cell fate is mainly determined by TCR signaling strength and inflammatory signals during priming[1,2]. We specify here that effector differentiation additionally depends on CD4$^+$ T-cell help that allows cDC1s to provide specific cytokine- and costimulatory signals to CD8$^+$ T cells[13–15,20]. We propose that the final differentiation fate of CD8$^+$ T cells is determined by the integration of TCR, costimulatory and cytokine signals received during both the first and the second priming steps. This would also explain why CTL responses are differentially dependent on CD4$^+$ T-cell help in diverse infection, tumor or vaccination settings, that vary in the amounts of antigen and inflammatory signals they elicit[24]. Our findings support that CD8$^+$ stem-like cells lie on the trajectory towards effector differentiation but can alternatively differentiate towards terminal exhaustion upon persistent antigen exposure, as recently suggested[7,10]. The fact that CD8$^+$ T-cell exhaustion in mouse models of chronic LCMV infection is exacerbated by CD4$^+$ T-cell depletion[26] fits in our concept that the stem-like cells that lie at the beginning of the exhaustion trajectory equal helpless cells.

Adoptive transfer showed that stem-like CD8$^+$ T cells formed after No Help vaccination could further proliferate and complete their CTL effector differentiation after Help vaccination. Ideally, CD4$^+$ T-cell help will improve the endogenous CD8$^+$ T-cell response in chronic infection and cancer. Adoptive transfer of virus-specific CD4$^+$ T cells in chronic LCMV infection indeed improved proliferative and cytotoxic capacities of stem-like CD8$^+$ T cells[27,28]. Also, adoptive transfer of neoantigen-specific CD4$^+$ T cells or expression of MHC-II-restricted neoantigens by tumor cells increased CTL activity and tumor control in mouse tumor models[48,49]. However, we found that expression of endogenous or exogenous helper epitopes by MC38 tumor cells failed to induce the helped CTL effector phenotype. The tumor-endogenous helper epitopes may have been too weak, since they also did not raise helped effector CD8$^+$ T cells outside the tumor context. Exogenous helper epitopes did increase the frequency of tumor-specific CD8$^+$ T cells raised, which likely contributed to the observed reduction in tumor outgrowth. MC38 cannot be directly recognized by CD4$^+$ T cells since it lacks MHC-II[29], but CD4$^+$ T cells may also have contributed indirectly via help to myeloid cells or B cells[50].

In the lymphocyte-depleted HPV-E7$^+$ TC-1 lung carcinoma model, raising a helped CTL response by therapeutic vaccination with our Help-E7 vaccine led to tumor control, while the No Help vaccine had no effect[20,29]. However, in the MC38 tumor context, where tumor-specific CD8$^+$ T cells are spontaneously primed, it appears challenging to transmit CD4$^+$ T-cell help signals. These findings are in line with a recent study showing that tumor-specific CD4$^+$ T cells raised by MC38 and other tumors acquire a dysfunctional state already in the dLN that is in part imposed by Tregs[51]. Tumors often lack inflammatory signals such as IFN-I and induce Treg responses[52,53], which attenuate DC activation and hamper delivery of CD4$^+$ T-cell help[12,19,51]. It will be of interest to understand the limitations and possibilities for delivery of help to the CTL response in cancers with different, defined TME types.

The validity of our CD8+ T-cell differentiation model should be further investigated in other settings, such as viral infection and human cancer. Nevertheless, we propose that helpless priming may be causally related to CD8+ T-cell exhaustion, since lack of helped effector CTLs will lead to antigen persistence[11]. We hope that our study contributes to a theoretical framework on CTL effector differentiation that provides a rationale to optimize immunotherapeutic strategies.

Methods

Mice

Female 8-10-week-old C57BL/6JRj mice obtained from Janvier Laboratories and OT-I (Tg(TcraTcrb)1100Mjb) mice on a CD45.1+ C57BL/6 background (bred in-house) were housed in individually ventilated cages under specific pathogen free conditions. Animal experiments were approved by the Experimental Animal Committee of Leiden University Medical Center and performed in accordance with national and European regulations. Cages were allocated randomly to experimental groups.

Vaccination

For intra-epidermal DNA vaccination, hair was removed from the right hind leg with depilating cream (Veet, Reckitt Benckiser) on day 0 and on days 0, 3, and 6, 15 µl of a 2 mg/ml plasmid DNA solution in H_2O was applied into the hairless skin of anesthetized mice with a Permanent Make Up tattoo device (Cheyenne, MT Derm GmbH), using a sterile disposable nine-needle bar with a needle depth of 1 mm and oscillating at a frequency of 100 Hz for 45 s, as described[26,27]. Plasmid DNA vaccines used were Help-E7SH (Help) and E7SH DNA (No Help)[29,30], OVA-Help and OVA-No Help[20], Rpl18-Adpgk-Help, and neoHelp and neoHelp-RA (Supplementary Methods).

Tumor challenge

The murine MC38-L colorectal carcinoma cell line was obtained from Leiden University Medical Center and has been characterized regarding neoepitope expression[44,45,54]. The MC38-Help cell line was created by transducing MC38-L cells with lentivirus encoding EF1a-Help-3xFLAG-IRES-eGFP (Supplementary Methods). Mice were injected subcutaneously in the right flank with 300.000 live MC38 or MC38-Help cells (LUMC) in 100 µl Hank's buffered salt solution (HBSS, Gibco). Tumor sizes were measured 3 times per week by caliper, and a tumor volume of 1000 mm^3 was maintained as humane endpoint.

Tissue processing and flow cytometry

Peripheral blood cells were obtained by tail vein bleeding in Microvette CB300 LH tubes (Sarstedt) and erythrocytes were removed by incubating twice in Red Blood Cell lysis buffer (Santa Cruz) for 1 min at room temperature. Spleens were passed through a 70 µm cell strainer (BD Falcon)

and erythrocytes were lysed for 5 min at room temperature. Right (dLN) and left (ndLN) inguinal LNs were digested into single cell suspensions with 100 µg/ml Liberase TL (Roche) in Dulbecco's Modified Eagle Medium (DMEM, Gibco) for 30 min at 37°C and passed through a 70 µm cell strainer. Tumors were isolated after perfusion of sacrificed mice with 15 ml phosphate buffered saline (PBS) with 2 mM ethylenediaminetetraacetic acid (EDTA, Santa Cruz). Tumors were mechanically disaggregated by scalpel and digested into single cell suspensions with 100 µg/ml Liberase TL (Roche) with 10 µg/ml DNAse I (Sigma) in DMEM (Gibco) for 30 min at 37°C. Tumors were passed through a 70 µm cell strainer. For flow cytometry, cells were washed with FACS buffer (PBS + 2% FCS) and stained for 1 h at room temperature with 1:200 PE-conjugated I-Ab/AKFVAAWTLKAA (PADRE) tetramers (NIH) or for 30 min on ice with 1:1000 LIVE/DEAD Near IR dye (Invitrogen) or 1:500 Zombie UV (Biolegend), 1:100 APC-conjugated H-2D^b/E7$_{49\text{-}57}$ tetramers, APC-conjugated H-2K^b/OVA$_{257\text{-}264}$ tetramers or APC-conjugated H-2K^b/KILTFDRL (mutated Rpl18) tetramers (produced in-house at LUMC) and monoclonal antibodies (mAbs) for surface staining (Supplementary Methods). For intracellular staining, cells were fixed and permeabilized with the FOXP3/transcription factor staining buffer set (eBioscience), according to the manufacturer's protocol and stained with antibodies for 30 min on ice (Supplementary Methods). Flow cytometry was performed using a 3-laser or 5-laser Aurora (Cytek) and SpectroFlow software.

Ex vivo restimulation

Ex vivo restimulation of splenocyte or tumor cell suspensions was performed as described [44]. In brief, cells of the DC line D1 were seeded in a 96-wells plate at 50.000 cells per well in conditioned medium and loaded with 1 mg/ml mutated Rpl18 and mutated Adpgk peptide or left unloaded, and incubated overnight at 37°C. The next day, 500.000 splenocytes or tumor cells were seeded on D1 cells and preincubated for 1 h at 37°C. Subsequently, GolgiPlug (BD Biosciences) was added at a final dilution of 1:1000 and left for 5 h at 37°C until analysis.

Adoptive cell transfer

OT-I CD8$^+$ T cells, carrying a transgenic Vα2/Vβ5 TCR recognizing OVA$_{257\text{-}264}$/H-2K^b, were isolated to more than 90% purity from spleens of naïve OT-I;CD45.1$^+$ C57BL/6 mice using a negative selection MACS CD8α$^+$ T-cell Isolation Kit (Miltenyi). OT-I cells were retro-orbitally (r.o.) injected at 10^5 cells per mouse into WT CD45.2$^+$ C57BL/6 mice on day -1, after which mice were vaccinated with OVA-No Help construct[20] on day 0, 3 and 6. On day 10, CD45.1$^+$ CD44$^+$ SLAMF6$^+$ helpless CD8$^+$ T cells were sorted from dLN on a 3-laser FACSAria II (BD Biosciences). Cells were r.o. injected at 10^4 cells per mouse into WT C57BL/6 mice, which were vaccinated once with OVA-Help or OVA-No Help on the next day.

Flow cytometry data analysis

Flow cytometry data were analyzed with OMIQ software and FlowAI[55] was used to remove events showing anomalies in flow rate, signal acquisition and dynamic range. After manual gating of tetramer$^+$ CD8$^+$ T cells (Supplementary Figure 1A) and conventional marker expression analysis,

subsampling was performed to select maximally 150 tetramer+ CD8+ T cells from each sample. Samples containing <5 total tetramer+ CD8+ T cells were excluded from further analysis. FlowSom[56] was used for K-means clustering of tetramer+ CD8+ T cells, including all markers except live/dead, CD4, CD8, FOXP3 and tetramer. Optimal t-distributed stochastic neighbor embedding (opt-SNE)[57] was used for dimension reduction and visualization of the data, using the same markers. Wanderlust[37] was used for trajectory analysis, using the same markers except Ki67, and using Cluster 10 (CD44-CD62L+ naive cells) as starting point. FlowSom clustering of all tetramer+ CD8+ cells from dLN at day 2-10 and 3 naïve LNs was done for the analysis of antigen-specific CD8+ T-cell populations on consecutive days after vaccination. Responding tetramer+ CD8+ T cells were selected for analysis by including clusters that showed <20% frequency in naïve LNs and a change in frequency between different time points after vaccination (Supplementary Figure 3D).

Statistical analysis

Data were analyzed with GraphPad Prism software using two-way ANOVA and Sidak's multiple comparisons test, unless indicated otherwise. Bars indicate means, error bars indicate SD. A P value < 0.05 was considered statistically significant; ns, not significant, *P < 0.05, **P < 0.005, ***P < 0.001 and ****P < 0.0001. Sample size was calculated a priori using G*Power software, using previous results of E7-specific CD8+ T-cell frequencies between Help and No Help[20] for power calculations.

Sample and library preparation for scRNAseq and TCRseq

Mice were vaccinated under Help or No Help conditions at day 0, 3, and 6 and were sacrificed at day 5 or day 10 after first vaccination, after which dLN and ndLN were isolated (Supplementary Figure 5). For each experimental condition, LNs from 3 individual mice were pooled to reduce biological variability, resulting in 8 samples (Supplementary Figure 6A). Samples were stained with the following mAbs: 1:100 CD19-PerCP/Vio700 (clone REA749, Miltenyi), 1:100 CD3-BV421 (clone 17A2, Biolegend), 1:100 CD44-PE/Cy7 (clone IM7, eBioscience), 1:100 CD62L-FITC (clone MEL-14, eBioscience). For each sample, activated T cells (CD19-CD3+CD44+CD62L-) were sorted on a 3-laser FACSAria II (BD Biosciences) and labeled with a distinct hashtag oligonucleotide (HTO)-conjugated mAb to MHC-I/CD45 (TotalSeq C0301 to C0307 and C0309, Biolegend), after which all 8 samples were pooled. scRNAseq libraries were prepared using a 10X Chromium single cell 5' v2 chemistry kit (10X Genomics) and TCRseq libraries were prepared using a 10X Chromium single cell V(D)J enrichment kit for mouse T cells (10X Genomics), according to the manufacturer's protocols. Sequencing was performed on a NovaSeq6000 system (Illumina). A total of 25,000 cells was used for sequencing, with a median sequencing depth of 11,196 reads per cell.

scRNAseq analysis

Analysis of scRNAseq and TCRseq data was performed using CellRanger (10X Genomics, v6.0.1) and Seurat (v4.3.0) in R (v4.2.3). For details, see Supplementary Methods. In summary, scRNAseq and TCRseq reads were aligned to the mouse reference genome mm10, TCR and BCR genes were

removed from the gene expression count matrix, and the dataset was analyzed using the standard Seurat pipeline. HTO demultiplexing was performed (Supplementary Figure 6B) and dataset was filtered based on number of RNA features, number of RNA counts, mitochondrial gene expression and expression of genes associated with B cells or APCs. Cell cycle scores for G2/M and S phase were assigned based on expression of G2/M and S phase genes, and these scores were regressed out during clustering. $CD8^+$ T-cell clusters were selected on presence of *Cd8a, Cd8b1* and absence of *Cd4* transcripts (Supplementary Figure 6C). Within the $CD8^+$ T-cell subset, number of cells per HTO was determined (Supplementary Figure 6D). HTOs containing <30 $CD8^+$ T cells were excluded from further analysis. Cluster 7, consisting of 52 $CD8^+$ T cells that showed only cell cycle genes as markers, was excluded, since cell cycle genes were regressed out during clustering. TCRseq analysis was performed using Loupe VDJ Browser (v5.0.0, 10X Genomics). Expanded clones were identified as TCR clonotypes containing 2 or more cells. TCR sequences from Loupe VDJ Browser, and UMAP projection and cluster annotation from Seurat were visualized together using Loupe Browser (v6.4.1, 10X Genomics). To quantify expanded clonotypes per differentiation cluster, only cells that grouped together in the UMAP with their assigned cluster were included. Seurat and Monocle3 (v1.3.1) in R were used for trajectory analysis. Ingenuity Pathway Analysis (Qiagen) was used for functional classification of differentially expressed genes between Cluster 2 and Cluster 3. For comparison of our scRNAseq data to published gene signatures, top 200 marker genes of TCF-1^+ progenitor (cluster 9) and effector (cluster 6) $CD8^+$ T cells from chronic and acute LCMV infection were downloaded from Table S5 from Pritykin *et al*. 2021[7]. These top 200 genes were used to calculate a module score for each cell in our dataset. The same method was performed using top 100 marker genes of stem-like $CD8^+$ T cells from the TdLN, (cluster 4) as published by Connolly *et al.* 2021[41], which were kindly provided to us by the authors.

Data availability

The scRNAseq and scTCRseq data utilized in Figure 4 have been deposited in the GEO database with the accession number GSE249046.

Acknowledgements

We thank Kees Franken for manufacturing tetramers, Mart de Boo for helping with tissue processing, Fiamma Salerno and Elselien Frijlink for scientific discussions, Ferry Ossendorp for advice on the tumor model, Susan Kloet for advise on scRNAseq, Tom de Wit for help with sorting, Evert de Vries for general support, Nikhil Yoshi and Kelli Connolly for sharing their dataset, and the Flow Cytometry Facility, Leiden Genome Technology Center, and Experimental Animal Facility of our institute for technical assistance.

Author Contributions

Study design: J.Bo, J.Bu; experimental design and performing experiments: J.Bu, D.B., M.S., Y.X, X.L; data analysis: J.Bu; manufacturing DNA vaccines: M.S.; paper writing: J.Bu, J.Bo; critical reading and editing of the paper: D.B., M.S., X.L, Y.X; supervision: J.Bo.

Competing Interests

The authors declare no competing financial interests in relation to the work described.

Funding

This research was supported by Oncode and grants 2017-11079 and 2017-10894 of the Dutch Cancer Society to J. Borst.

References

1. Henning, A. N., Roychoudhuri, R. & Restifo, N. P. Epigenetic control of CD8+ T cell differentiation. *Nat. Rev. Immunol.* **18**, 340–356 (2018).
2. Kaech, S. M. & Cui, W. Transcriptional control of effector and memory CD8 + T cell differentiation. *Nat. Rev. Immunol.* **12**, 749–761 (2012).
3. Philip, M. & Schietinger, A. CD8+ T cell differentiation and dysfunction in cancer. *Nat. Rev. Immunol.* **22**, 209–223 (2022).
4. Gebhardt, T., Park, S. L. & Parish, I. A. Stem-like exhausted and memory CD8+ T cells in cancer. *Nat. Rev. Cancer* **23**, 780–798 (2023).
5. Zehn, D., Thimme, R., Lugli, E., de Almeida, G. P. & Oxenius, A. 'Stem-like' precursors are the fount to sustain persistent CD8+ T cell responses. *Nat. Immunol.* **23**, 836–847 (2022).
6. Chow, A., Perica, K., Klebanoff, C. A. & Wolchok, J. D. Clinical implications of T cell exhaustion for cancer immunotherapy. *Nat. Rev. Clin. Oncol.* **19**, 775–790 (2022).
7. Pritykin, Y. *et al.* A unified atlas of CD8 T cell dysfunctional states in cancer and infection. *Mol. Cell* **81**, 2477–2493 (2021).
8. Zheng, L. *et al.* Pan-cancer single-cell landscape of tumor-infiltrating T cells. *Science (1979).* **374**, 6474 (2021).
9. Broomfield, B. J. & Groom, J. R. Defining the niche for stem-like CD8+ T cell formation and function. *Curr. Opin. Immunol.* **89**, 102454 (2024).
10. McManus, D. T. *et al.* An early precursor CD8+ T cell that adapts to acute or chronic viral infection. *Nature* **640**, 772–781 (2025).

11. Busselaar, J., Tian, S., van Eenennaam, H. & Borst, J. Helpless Priming Sends CD8+ T Cells on the Road to Exhaustion. *Front. Immunol.* **11**, 592569 (2020).

12. Busselaar, J., Sijbranda, M. & Borst, J. The importance of type I interferon in orchestrating the cytotoxic T-cell response to cancer. *Immunol. Lett.* **270**, 106938 (2024).

13. Wu, R. & Murphy, K. M. DCs at the center of help: Origins and evolution of the three-cell-type hypothesis. *Journal of Experimental Medicine* **219**, 1–13 (2022).

14. Borst, J., Ahrends, T., Bąbała, N., Melief, C. J. M. & Kastenmüller, W. CD4+ T cell help in cancer immunology and immunotherapy. *Nat. Rev. Immunol.* **18**, 635–647 (2018).

15. Ferris, S. T. *et al.* cDC1 prime and are licensed by CD4+ T cells to induce anti-tumour immunity. *Nature* **584**, 624–629 (2020).

16. Lei, X. *et al.* CD4+ helper T cells endow cDC1 with cancer-impeding functions in the human tumor micro-environment. *Nat. Commun.* **14**, 217 (2023).

17. Lei, X. *et al.* CD4+ T cells produce IFN-I to license cDC1s for induction of cytotoxic T-cell activity in human tumors. *Cell. Mol. Immunol.* 1–19 (2024) doi:10.1038/s41423-024-01133-1.

18. Wu, R. *et al.* Mechanisms of CD40-dependent cDC1 licensing beyond costimulation. *Nat. Immunol.* **23**, 1536–1550 (2022).

19. Gressier, E. *et al.* CD4+ T cell calibration of antigen-presenting cells optimizes antiviral CD8+ T cell immunity. *Nat. Immunol.* **24**, (2023).

20. Ahrends, T. *et al.* CD4+ T cell help confers a cytotoxic T cell effector program including coinhibitory receptor downregulation and increased tissue invasiveness. *Immunity* **47**, 848–861 (2017).

21. Ahrends, T. *et al.* CD4+ T cell help creates memory CD8+ T cells with innate and help-independent recall capacities. *Nat. Commun.* **10**, 5531 (2019).

22. Provine, N. M. *et al.* Immediate dysfunction of vaccine-elicited CD8 + T cells primed in the absence of CD4 + T cells. *The Journal of Immunology* **197**, 1809–1822 (2016).

23. Brewitz, A. *et al.* CD8+T cells orchestrate pDC-XCR1+dendritic cell spatial and functional cooperativity to optimize priming. *Immunity* **46**, 205–219 (2017).

24. Wiesel, M. & Oxenius, A. From crucial to negligible: Functional CD8+ T-cell responses and their dependence on CD4+ T-cell help. *Eur. J. Immunol.* **42**, 1080–1088 (2012).

25. Jobin, K. *et al.* A distinct priming phase regulates CD8 T cell immunity by orchestrating paracrine IL-2 signals. *Science (1979).* **388**, (2025).

26. Wherry, E. J. *et al.* Molecular Signature of CD8+ T Cell Exhaustion during Chronic Viral Infection. *Immunity* **27**, 670–684 (2007).

27. Kanev, K. *et al.* Proliferation-competent Tcf1+ CD8 T cells in dysfunctional populations are CD4 T cell help independent. *Proc. Natl. Acad. Sci. U. S. A.* **116**, 20070–20076 (2019).

28. Zander, R. *et al.* CD4+ T Cell Help Is Required for the Formation of a Cytolytic CD8+ T Cell Subset that Protects against Chronic Infection and Cancer. *Immunity* **51**, 1028–1042 (2019).

29. Ahrends, T. *et al.* CD27 Agonism Plus PD-1 Blockade Recapitulates CD4+ T-cell Help in Therapeutic Anticancer Vaccination. *Cancer Res.* **76**, 2921–2931 (2016).

30. Oosterhuis, K., Aleyd, E., Vrijland, K., Schumacher, T. N. & Haanen, J. B. Rational design of DNA vaccines for the induction of human papillomavirus type 16 E6-and E7-specific cytotoxic T-cell responses. *Hum. Gene Ther.* **23**, 3001–1312 (2012).

31. Babala, N. *et al.* Subcellular Localization of Antigen in Keratinocytes Dictates Delivery of CD4 + T-cell Help for the CTL Response upon Therapeutic DNA Vaccination into the Skin. *Cancer Immunol. Res.* **6**, 835–847 (2018).

32. Bins, A. D. *et al.* A rapid and potent DNA vaccination strategy defined by in vivo monitoring of antigen expression. *Nat. Med.* **11**, 899–904 (2005).

33. Schenkel, J. M. *et al.* Conventional type I dendritic cells maintain a reservoir of proliferative tumor-antigen specific TCF-1+ CD8+ T cells in tumor-draining lymph nodes. *Immunity* **54**, 2338–2353 (2021).

34. Gattinoni, L., Speiser, D. E., Lichterfeld, M. & Bonini, C. T memory stem cells in health and disease. *Nat. Med.* **23**, 18–27 (2017).

35. Joshi, N. S. *et al.* Inflammation Directs Memory Precursor and Short-Lived Effector CD8+ T Cell Fates via the Graded Expression of T-bet Transcription Factor. *Immunity* **27**, 281–295 (2007).

36. Gerlach, C. *et al.* The Chemokine Receptor CX3CR1 Defines Three Antigen-Experienced CD8 T Cell Subsets with Distinct Roles in Immune Surveillance and Homeostasis. *Immunity* **45**, 1270–1284 (2016).

37. Bendall, S. C. *et al.* Single-Cell Trajectory Detection Uncovers Progression and Regulatory Coordination in Human B cell Development. *Cell* **157**, 714 (2014).

38. Siddiqui, I. *et al.* Intratumoral Tcf1+PD-1+CD8+ T cells with stem-like properties promote tumor control in response to vaccination and checkpoint blockade immunotherapy. *Immunity* **50**, 195–211 (2019).

39. Beltra, J.-C. *et al.* Developmental relationships of four exhausted CD8+ T Cell subsets reveals underlying transcriptional and epigenetic landscape control mechanisms. *Immunity* **52**, 825–841 (2020).

40. Trapnell, C. *et al.* The dynamics and regulators of cell fate decisions are revealed by pseudotemporal ordering of single cells. *Nat. Biotechnol.* **32**, 381–386 (2014).

41. Connolly, K. A. *et al.* A reservoir of stem-like CD8 + T cells in the tumor-draining lymph node preserves the ongoing antitumor immune response. *Sci. Immunol.* **6**, 64 (2021).

42. Frijlink, E. *et al.* PD-1 or CTLA-4 blockade promotes CD86-driven Treg responses upon radiotherapy of lymphocyte-depleted cancer in mice. *Journal of Clinical Investigation* **134**, (2024).

43. Yadav, M. *et al.* Predicting immunogenic tumour mutations by combining mass spectrometry and exome sequencing. *Nature* **515**, 572–576 (2014).

44. Hos, B. J. *et al.* Identification of a neo-epitope dominating endogenous CD8 T cell responses to MC-38 colorectal cancer. *Oncoimmunology* **9**, e1673125 (2020).

45. Hos, B. J. *et al.* Cancer-specific T helper shared and neo-epitopes uncovered by expression of the MHC class II master regulator CIITA. *Cell Rep.* **41**, 111485 (2022).

46. Johnnidis, J. B. *et al.* Inhibitory signaling sustains a distinct early memory CD8+ T cell precursor that is resistant to DNA damage. *Sci. Immunol.* **6**, (2021).

47. Pais Ferreira, D. *et al.* Central memory CD8+ T cells derive from stem-like Tcf7hi effector cells in the absence of cytotoxic differentiation. *Immunity* **53**, 985–1000 (2020).

48. Brightman, S. E. *et al.* Neoantigen-specific stem cell memory-like CD4+ T cells mediate CD8+ T cell-dependent immunotherapy of MHC class II-negative solid tumors. *Nat. Immunol.* **24**, 1345–1357 (2023).

49. Alspach, E. *et al.* MHC-II neoantigens shape tumour immunity and response to immunotherapy. *Nature* **574**, 696–701 (2019).

50. Speiser, D. E., Chijioke, O., Schaeuble, K. & Münz, C. CD4+ T cells in cancer. *Nat. Cancer* **4**, 317–329 (2023).

51. Guo, M. *et al.* Molecular, metabolic, and functional CD4 T cell paralysis in the lymph node impedes tumor control. *Cell Rep.* **42**, 113047 (2023).

52. Luca, B. A. *et al.* Atlas of clinically distinct cell states and ecosystems across human solid tumors. *Cell* **184**, 5482–5496 (2021).

53. Combes, A. J. *et al.* Discovering dominant tumor immune archetypes in a pan-cancer census. *Cell* **185**, 184–203 (2022).

54. Schrörs, B. *et al.* MC38 colorectal tumor cell lines from two different sources display substantial differences in transcriptome, mutanome and neoantigen expression. *Front. Immunol.* **14**, (2023).

55. Monaco, G. *et al.* flowAI: automatic and interactive anomaly discerning tools for flow cytometry data. *Bioinformatics* **32**, 2473–2480 (2016).

56. Van Gassen, S. *et al.* FlowSOM: Using self-organizing maps for visualization and interpretation of cytometry data. *Cytometry Part A* **87**, 636–645 (2015).

57. Belkina, A. C. *et al.* Automated optimized parameters for T-distributed stochastic neighbor embedding improve visualization and analysis of large datasets. *Nat. Commun.* **10**, 5415 (2019).

Supplementary Figures

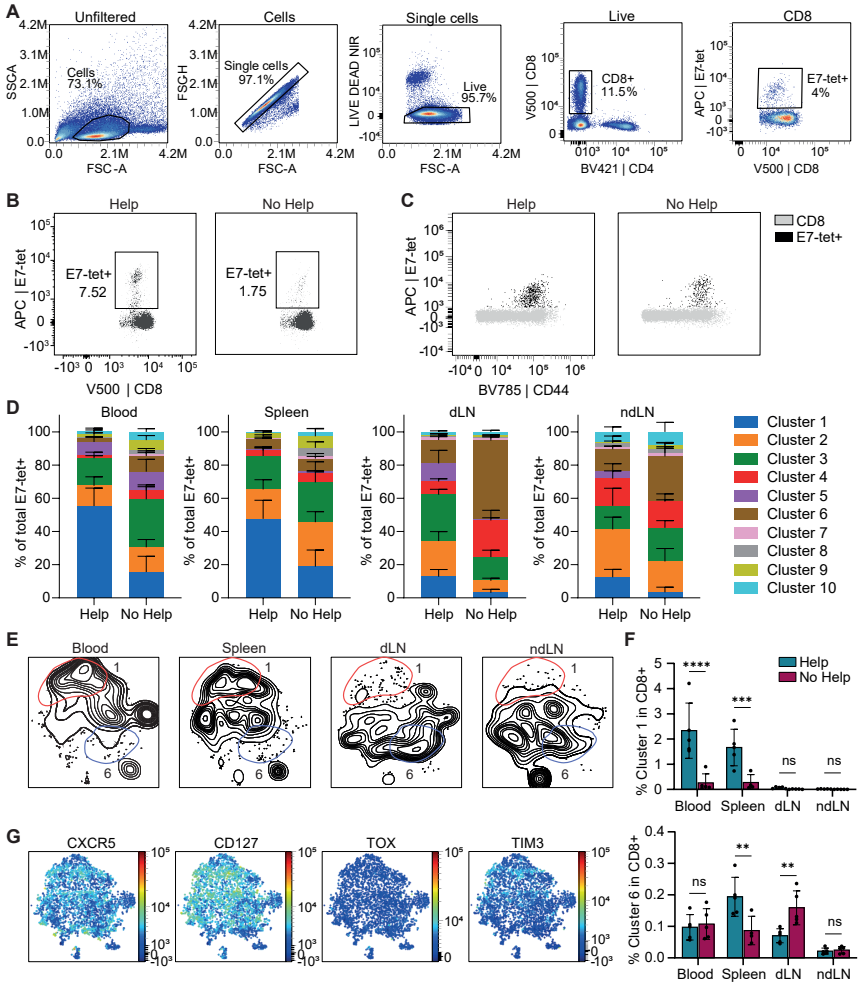

Supplementary Figure 1. Gating and phenotyping of antigen-specific CD8⁺ T cells after Help and No Help vaccination. Mice were vaccinated under Help or No Help conditions at day 0, 3, and 6 and sacrificed at day 10 after which blood, spleen, dLN and ndLN were analyzed as described in Figure 1. (A) Gating strategy for antigen-specific (E7-tetramer⁺) CD8⁺ T cells at day 10 after vaccination. Gating strategy is shown for 1 blood sample, but was used consistently for all experiments and organs. (B-C) Representative FACS plots from one mouse per group, showing E7-tetramer⁺ CD8⁺ cells in blood at day 11 after vaccination (B) and CD44 expression in E7-tet⁺ and total CD8⁺ in spleen at day 10 (C). (D-G) Opt-SNE visualization and FlowSom clustering of E7-tetramer⁺ CD8⁺ T cells at day 10 after Help or No Help vaccination was performed as shown in Figure 1E. (D) Frequency of tetramer⁺ CD8⁺ T cells per cluster per organ. (E) Distribution of cells from different organs across opt-SNE. (F) Frequency of Cluster 1 and Cluster 6 E7-tetramer+ cells in total CD8+ T cells per organ after Help versus No Help vaccination. (G) Expression of additional differentiation markers on cumulative E7-tetramer⁺ CD8⁺ T cells from all experimental settings visualized by opt-SNE. Data are from 1 experiment, representative of 2 independent experiments with n=5 mice per group. ns, not significant, **P <0.005, ***P < 0.001 and ****P < 0.0001.

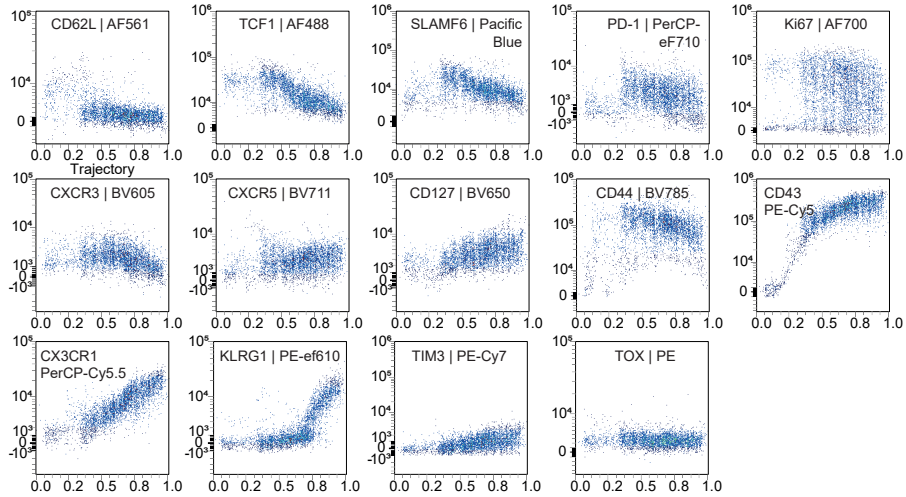

Supplementary Figure 2. Expression of marker proteins along the CTL differentiation spectrum upon vaccination. Antigen-specific E7-tetramer$^+$ CD8$^+$ T cells from blood, spleen, dLN and ndLN at day 10 after Help or No Help vaccination were analyzed by flow cytometry using the differentiation marker panel, as shown in Figure 2. FACS plots showing expression levels of each differentiation marker against the Wanderlust trajectory score. Data are from 1 experiment, representative of 2 independent experiments with n=5 mice per group.

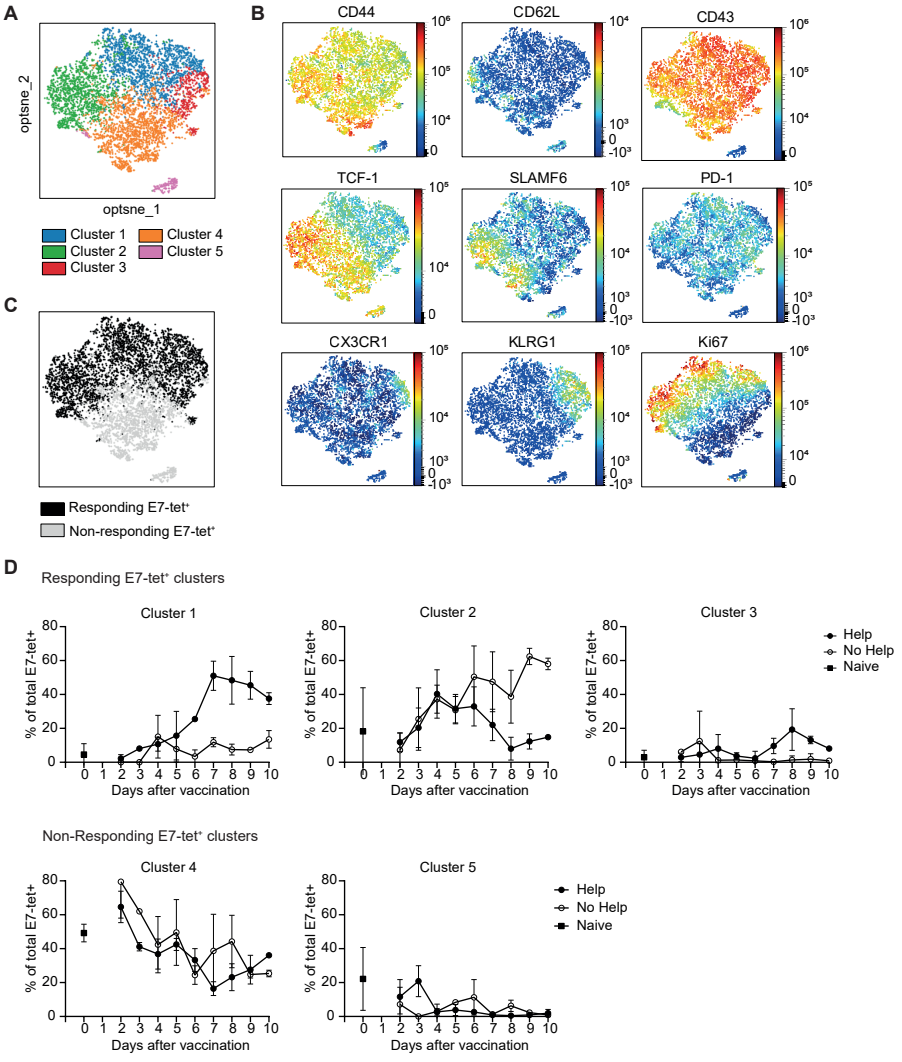

Supplementary Figure 3. Selection of responding E7-tetramer⁺ clusters for analysis over time. Experimental details related to the timecourse experiment depicted in Figure 3. Mice received Help or No Help vaccination at day 0, 3 and 6, and different cohorts of mice were sacrificed at day 2-10 after first vaccination (A) Opt-SNE dimension reduction and FlowSom clustering of E7-tetramer⁺ CD8⁺ T cells form dLN of vaccinated mice (n=3 per group per timepoint), and 3 naive LNs. (B) Expression of differentiation markers on cumulative E7-tetramer⁺ CD8⁺ T cells from all experimental settings visualized by opt-SNE. (C) Responding and non-responding E7-tetramer⁺ CD8⁺ T cells in opt-SNE. (D) Frequencies of responding E7-tetramer⁺ clusters and non-responding E7-tetramer⁺ clusters in naive LNs and at different timepoints after vaccination. Responding clusters were determined by a frequency of <20% in naive LN, and a change in frequency between different timepoints after vaccination. Responding E7-tetramer⁺ CD8⁺ T cells from vaccinated mice (day 2-10) were used for further analysis as shown in Figure 3.

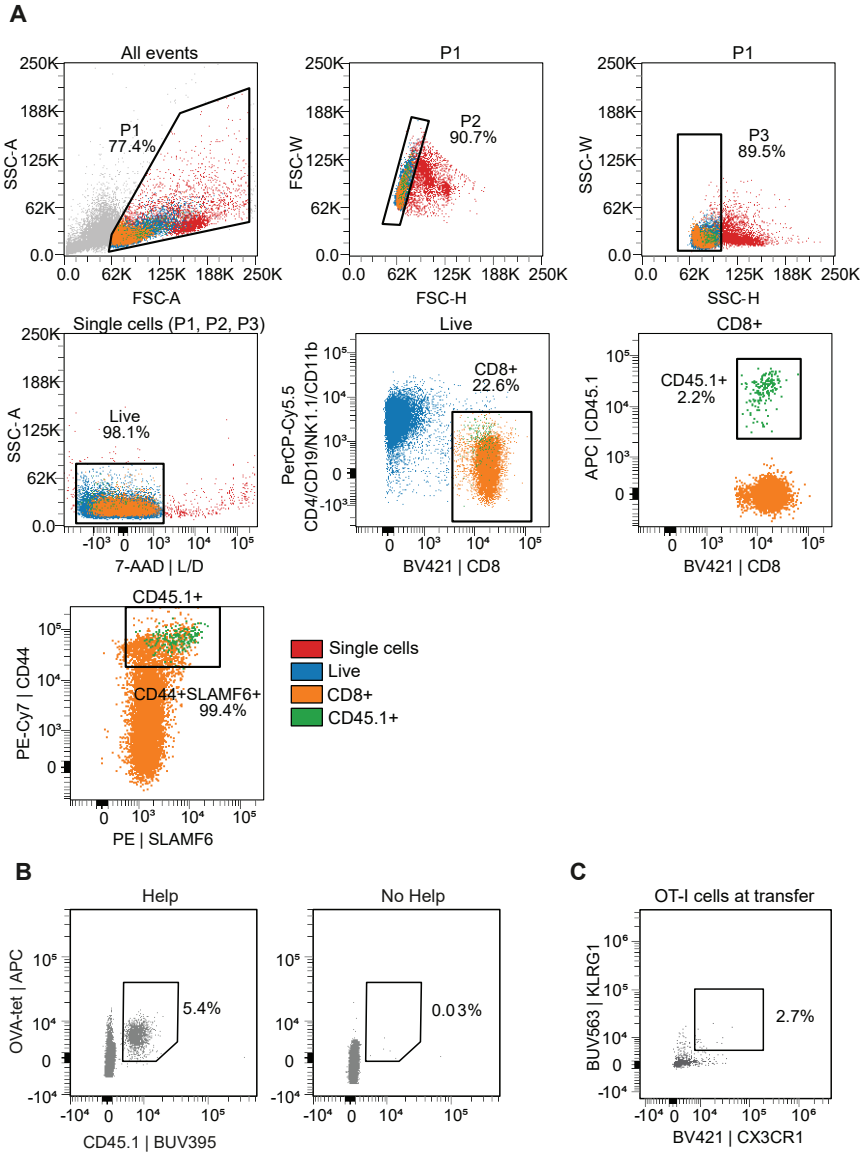

Supplementary Figure 4. Adoptive transfer of helpless OT-I cells. Naïve CD45.1$^+$ $OVA_{257/264}$/H-2K^b-specific OT-I cells were adoptively transferred to CD45.2$^+$ recipient mice, which were subsequently vaccinated with No Help vaccine encoding the $OVA_{257/264}$ epitope, as shown in Figure 3. (A) Sorting strategy of CD44$^+$SLAM-F6$^+$CD45.1$^+$CD8$^+$ (OT-I) T cells from dLN at day 10 after vaccination of the primary recipient mice. Sorting was performed on pooled dLNs from 5 mice and these cells were used for adoptive transfer into secondary CD45.2$^+$ recipient mice. (B) Representative FACS plots from one mouse per group, showing OT-I cells in blood at day 21, which is day 10 after secondary recipient vaccination. (C) Manual gating of KLRG1$^+$CX3CR1$^+$ effector cells within the pooled population of OT-I cells before transfer to secondary recipients.

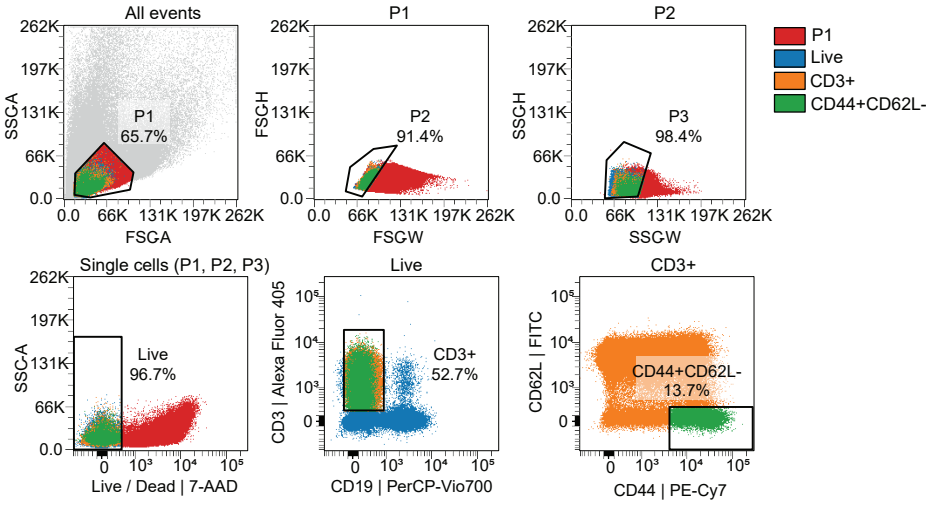

Supplementary Figure 5. Sorting strategy of activated T cells for scRNAseq. Sorting strategy for the scRNAseq experiment depicted in Figure 4. Mice were vaccinated under E7-Help or No Help conditions (n=3 per group) and activated T cells were flow cytometrically sorted per experimental group from pooled dLN or ndLN at day 5 or day 10, on a $CD3^{+}CD44^{+}CD62L^{-}$ phenotype.

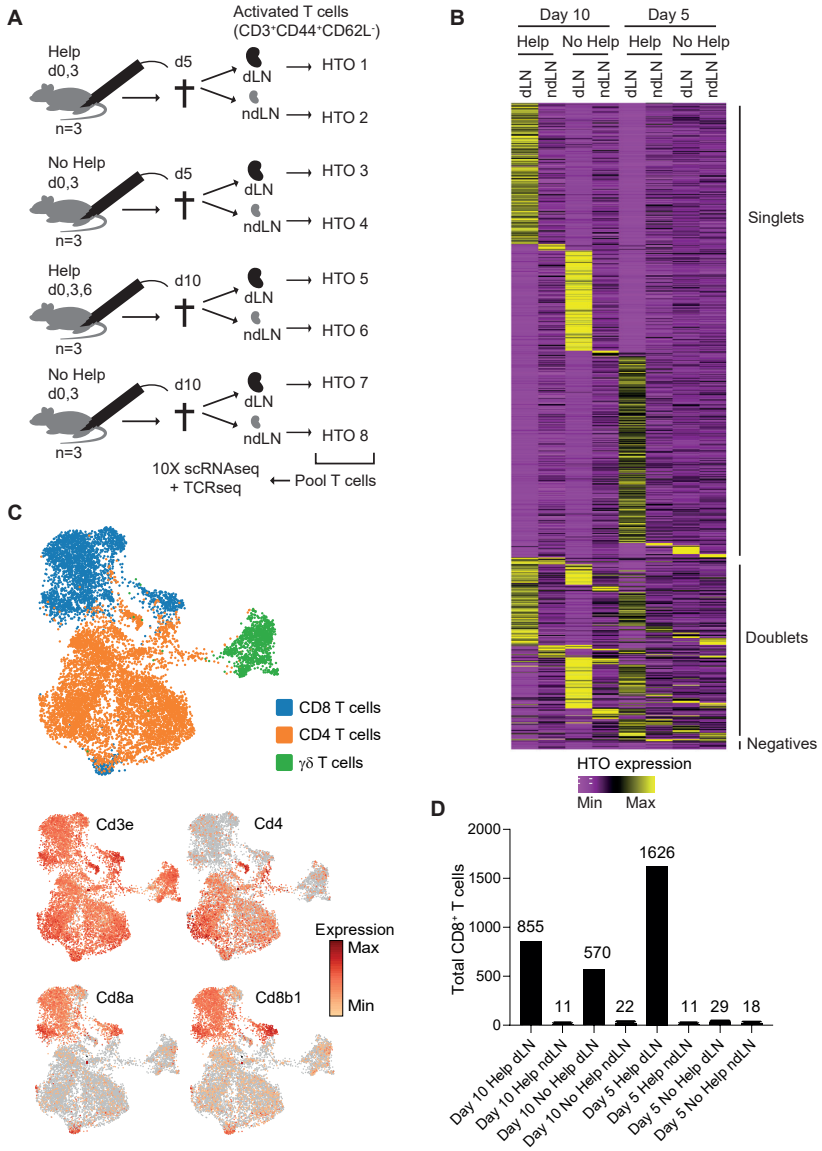

Supplementary Figure 6. Generation and processing of scRNAseq data of CD8⁺ T cells after Help or No Help vaccination. Experimental details related to the scRNAseq experiment depicted in Figure 4. (A) Experimental setup. Mice (n=3 per group) received E7-Help or No Help vaccination at the indicated days and were sacrificed at day 5 or day 10, after which dLN and ndLN were isolated and pooled per group. Activated T cells were sorted and labeled with MHC-II/CD45 antibody-coupled hashtag oligonucleotide (HTO) as indicated. T cells from all HTO groups were pooled and subjected to 10x Genomics scRNAseq, coupled to TCRseq. (B) Heatmap showing HTO demultiplexing results. The color scale indicates expression levels of HTO corresponding to each experimental condition per cell. (C) Expression of canonical T cell marker genes across UMAP of activated T cells, for identification of CD8⁺, CD4⁺ and γδT cells.(D) Number of CD8⁺ T cells per experimental condition after the entire procedure, as identified by HTO expression level.

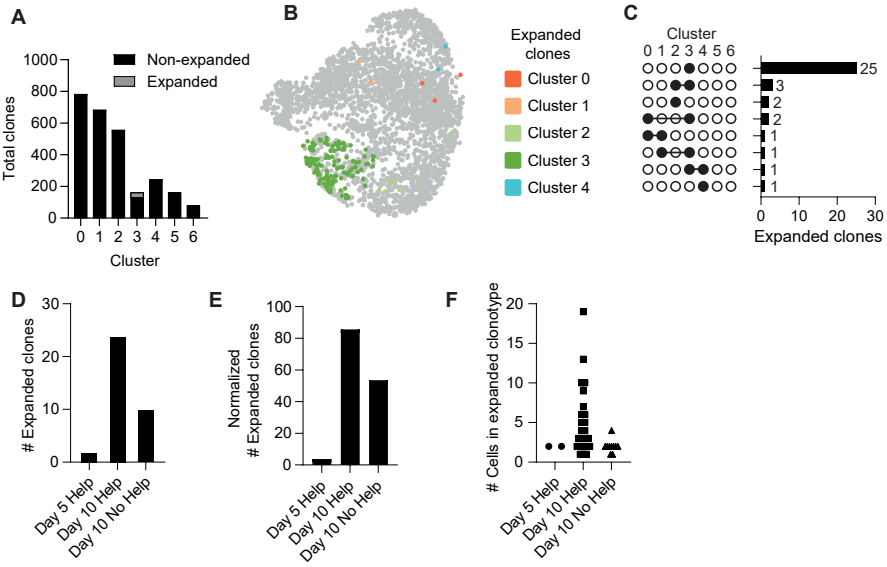

Supplementary Figure 7. Quantification and characterization of expanded TCR clones within CD8⁺ T cells after vaccination under Help or No Help conditions. Experimental details related to the TCRseq analysis depicted in Figure 4. (A) Quantification of distinct TCR clones that are non-expanded (containing 1 cell) or expanded (containing 2 or more cells) in each of the CD8⁺ T cell clusters identified in Figure 4A. (B) UMAP showing CD8⁺ T cells from expanded clones per CD8⁺ T cell cluster. (C) Number of unique expanded TCR clones, of which all cells are found within one cluster (indicated by one black circle), and shared TCR clones, containing cells that are found in multiple clusters (indicated by multiple connected black circles). (D, E) Number of expanded TCR clones per experimental condition, absolute (D) and normalized to number of cells per condition (E). (F) Number of cells belonging to each expanded clonotype per experimental condition.

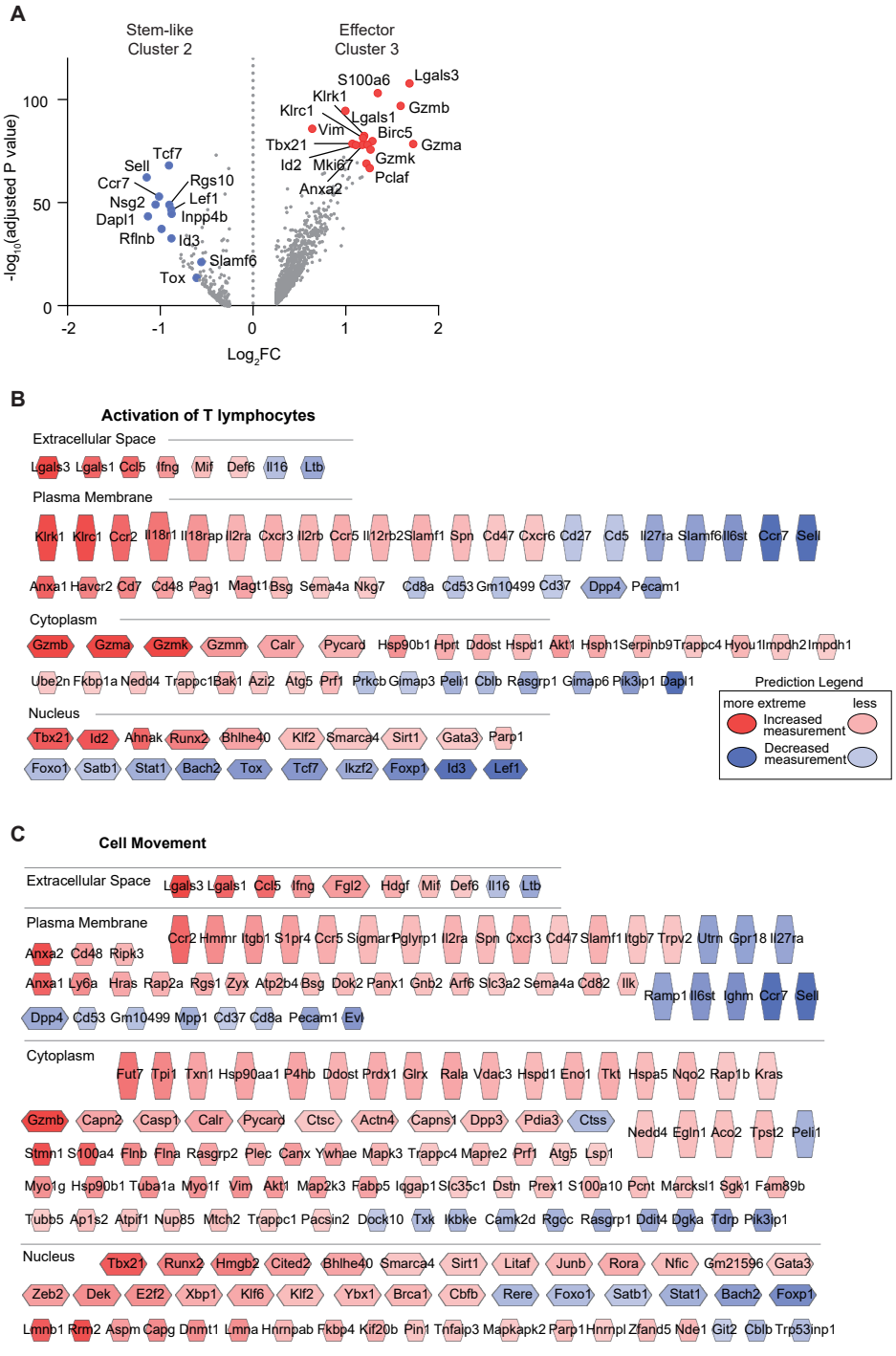
A
Stem-like
Cluster 2
Effector
Cluster 3
-log10(adjusted P value)
Log2FC
Tcf7
Sell
Ccr7
Rgs10
Nsg2
Lef1
Dapl1
Inpp4b
Rflnb
Id3
Slamf6
Tox
S100a6
Lgals3
Klrk1
Klrc1
Gzmb
Lgals1
Vim
Birc5
Tbx21
Gzma
Id2
Mki67
Gzmk
Pclaf
Anxa2
B
Activation of T lymphocytes
Extracellular Space
Lgals3 Lgals1 Ccl5 Ifng Mif Def6 Il16 Ltb
Plasma Membrane
Klrk1 Klrc1 Ccr2 Il18r1 Il18rap Il2ra Cxcr3 Il2rb Ccr5 Il12rb2 Slamf1 Spn Cd47 Cxcr6 Cd27 Cd5 Il27ra Slamf6 Il6st Ccr7 Sell
Anxa1 Havcr2 Cd7 Cd48 Pag1 Magt1 Bsg Sema4a Nkg7 Cd8a Cd53 Gm10499 Cd37 Dpp4 Pecam1
Cytoplasm
Gzmb Gzma Gzmk Gzmm Calr Pycard Hsp90b1 Hprt Ddost Hspd1 Akt1 Hsph1 Serpinb9 Trappc4 Hyou1 Impdh2 Impdh1
Ube2n Fkbp1a Nedd4 Trappc1 Bak1 Azi2 Atg5 Prf1 Prkcb Gimap3 Peli1 Cblb Rasgrp1 Gimap6 Pik3ip1 Dapl1
Nucleus
Tbx21 Id2 Ahnak Runx2 Bhlhe40 Klf2 Smarca4 Sirt1 Gata3 Parp1
Foxo1 Satb1 Stat1 Bach2 Tox Tcf7 Ikzf2 Foxp1 Id3 Lef1
Prediction Legend
more extreme
less
Increased measurement
Decreased measurement
C
Cell Movement
Extracellular Space
Lgals3 Lgals1 Ccl5 Ifng Fgl2 Hdgf Mif Def6 Il16 Ltb
Plasma Membrane
Anxa2 Cd48 Ripk3
Ccr2 Hmmr Itgb1 S1pr4 Ccr5 Sigmar1 Plgrp1 Il2ra Spn Cxcr3 Cd47 Slamf1 Itgb7 Trpv2 Utrn Gpr18 Il27ra
Anxa1 Ly6a Hras Rap2a Rgs1 Zyx Atp2b4 Bsg Dok2 Panx1 Gnb2 Arf6 Slc3a2 Sema4a Cd82 Ilk
Ramp1 Il6st Ighm Ccr7 Sell
Dpp4 Cd53 Gm10499 Mpp1 Cd37 Cd8a Pecam1 Evl
Cytoplasm
Fut7 Tpi1 Txn1 Hsp90aa1 P4hb Ddost Prdx1 Glrx Rala Vdac3 Hspd1 Eno1 Tkt Hspa5 Nqo2 Rap1b Kras
Gzmb Capn2 Casp1 Calr Pycard Ctsc Actn4 Capns1 Dpp3 Pdia3 Ctss
Nedd4 Egln1 Aco2 Tpst2 Peli1
Stmn1 S100a4 Flnb Flna Rasgrp2 Plec Canx Ywhae Mapk3 Trappc4 Mapre2 Prf1 Atg5 Lsp1
Myo1g Hsp90b1 Tuba1a Myo1f Vim Akt1 Map2k3 Fabp5 Iqgap1 Slc35c1 Dstn Prex1 S100a10 Pcnt Marcksl1 Sgk1 Fam89b
Tubb5 Ap1s2 Atpif1 Nup85 Mtch2 Trappc1 Pacsin2 Dock10 Txk Ikbke Camk2d Rgcc Rasgrp1 Ddit4 Dgka Tdrp Pik3ip1
Nucleus
Tbx21 Runx2 Hmgb2 Cited2 Bhlhe40 Smarca4 Sirt1 Litaf Junb Rora Nfic Gm21596 Gata3
Zeb2 Dek E2f2 Xbp1 Klf6 Klf2 Ybx1 Brca1 Cbfb Rere Foxo1 Satb1 Stat1 Bach2 Foxp1
Lmnb1 Rrm2 Aspm Capg Dnmt1 Lmna Hnrnpab Fkbp4 Kif20b Pin1 Tnfaip3 Mapkapk2 Parp1 Hnrnpl Zfand5 Ndel1 Git2 Cblb Trp53inp1

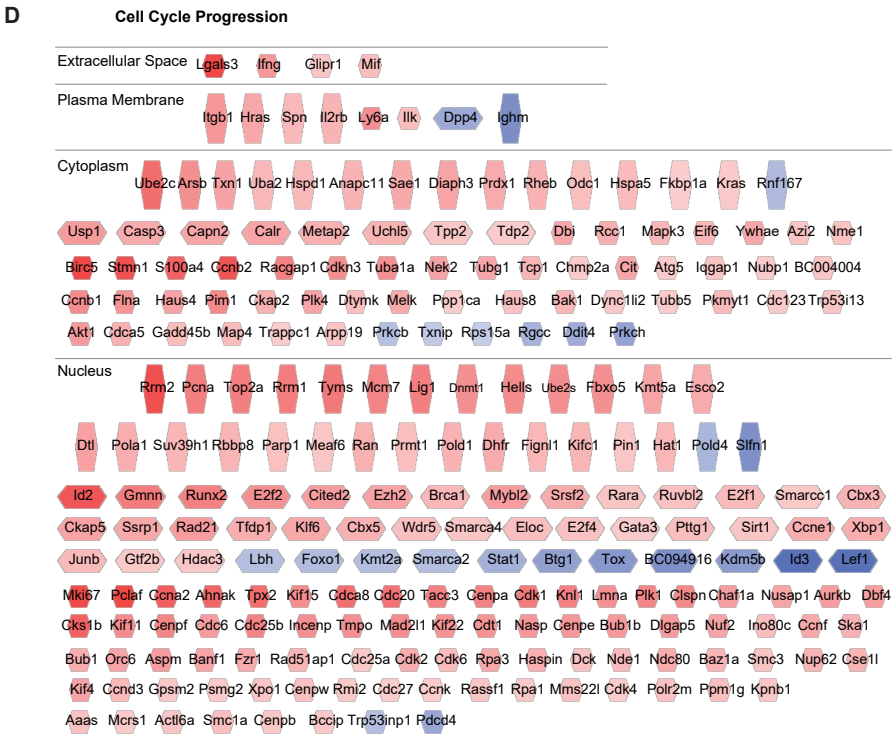

Supplementary Figure 8. Functional differences between effector and stem-like CD8⁺ T cells. (A) Volcano plot showing genes that are differentially expressed between Cluster 2 and Cluster 3. (B-D) Ingenuity Pathway Analysis (IPA) showing transcripts in the category "Activation of T lymphocytes" (B), "Cell Movement" (C) and "Cell Cycle Progression" (D), with high (red) or low (blue) expression levels in helped effector Cluster 3 as compared to stem-like Cluster 2.

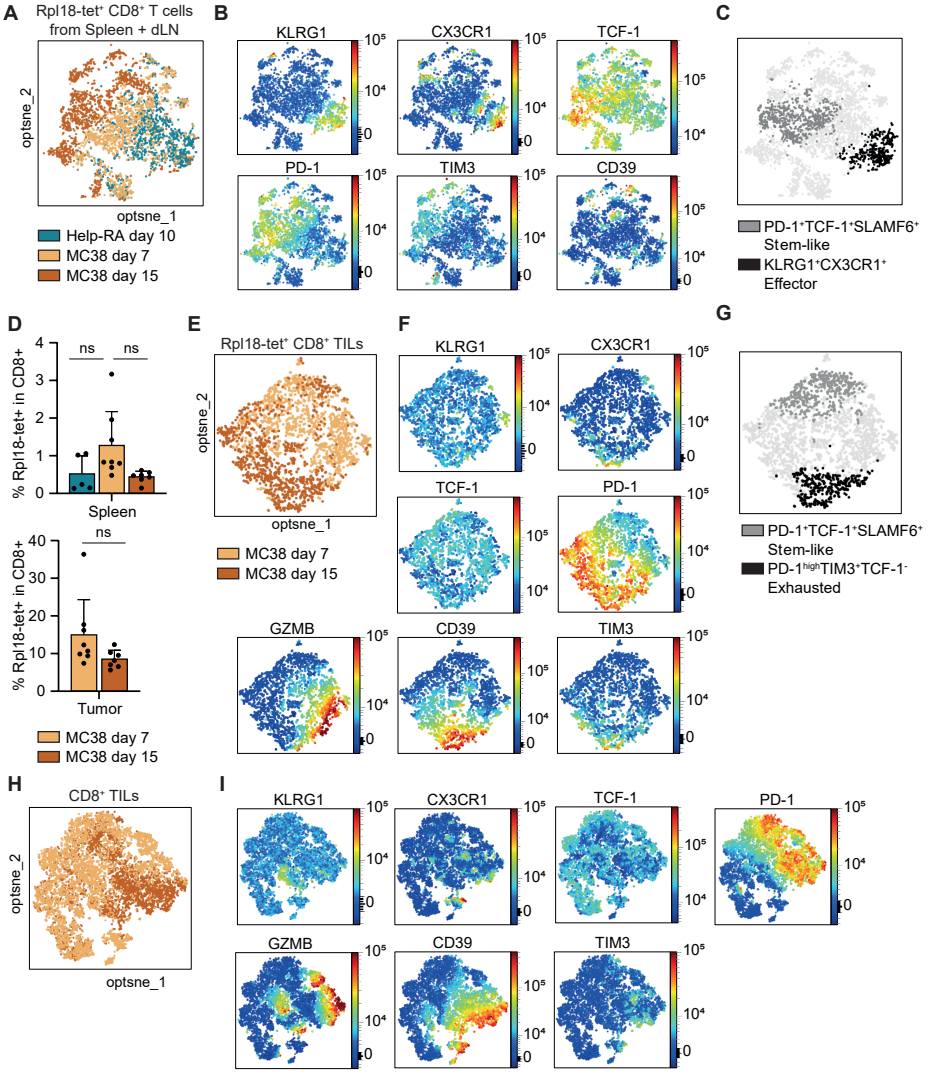

Supplementary Figure 9. Characterization of antigen-specific CD8+ T cells raised after vaccination or tumor implantation. (A) Opt-SNE visualization of Rpl18-tetramer+ CD8+ T cells from spleen and dLN after Help-RA vaccination or MC38 tumor implantation, as described in Figure 6. (B) Expression of differentiation markers on cumulative Rpl18-tetramer+ CD8+ T cells in spleen and dLN from the experimental settings visualized by opt-SNE in panel A. (C) Visualization of the PD-1+TCF-1+ stem-like and KLRG1+CX3CR1+ effector populations within opt-SNE. (D) Percentage of Rpl18-tetramer+ CD8+ T cells in spleen and the MC38 tumor, in the experiment depicted in Figure 7E-M. (E) Opt-SNE visualization of Rpl18-tetramer+ CD8+ TILs harvested from MC38 tumors at days 7 or day 15.(F) Expression of differentiation markers on cumulative Rpl18-tetramer+ CD8+ TILs visualized by opt-SNE. (G) Visualization of the PD-1hiTIM3+TCF-1- exhausted and PD-1+TCF-1+ stem-like populations within opt-SNE. (H) Opt-SNE visualization of total CD8+ TILs harvested from MC38 tumors at days 7 or day 15. (I) Expression of differentiation markers on cumulative total CD8+ TILs visualized by opt-SNE.

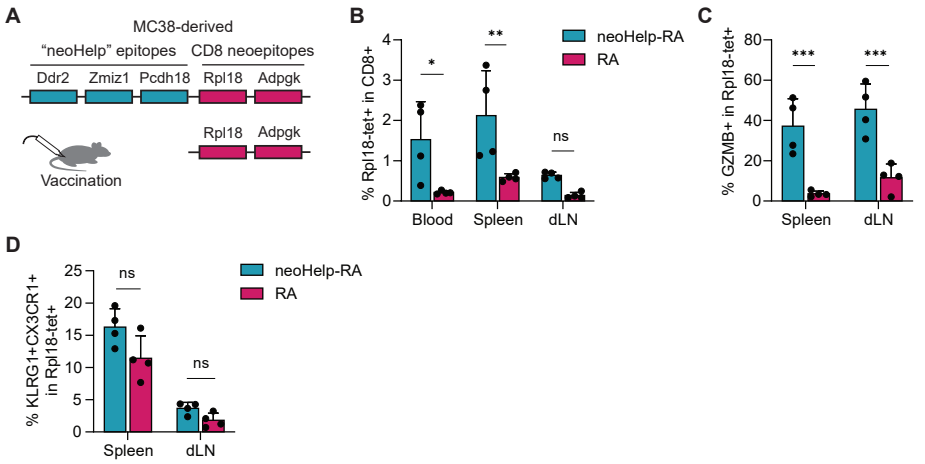

Supplementary Figure 10. Vaccination with neoHelp epitopes improves MC38-specific CTL response outside tumor context. (A) Experimental setup. Mice were vaccinated on day 0, 3 and 6 with DNA construct encoding the MC38-derived MHC-I restricted neoeptiopes mutated Rpl18 and Adpgk (RA), either alone or in conjunction with MC38-derived MHC-II restriced neoepitopes mutated Ddr2, Zmiz1 and Pcdh18 (neoHelp-RA). On day 10, mice were sacrificed and Rpl18-specifc (tet⁺) CD8⁺ T-cell responses were assessed.(B) Frequency of Rpl18-tetramer⁺ CD8⁺ T cells in indicated tissues on day 10. (C, D) Frequency of Granzyme-B (GZMB)⁺ cells (C) or KLRG1⁺CX3CR1⁺ effector cells (D) within the Rpl18-specific CD8⁺ T cell population in spleen and dLN. Data are from 1 experiment representative of 2 independent experiments, with n=4 mice per group. Error bars indicate SD. Statistical significance was calulated by two-way ANOVA and Sidak's multiple comparsions test. ns, non significant, *P < 0.05, **P < 0.005 and ***P < 0.001.

Description of Supplementary Tables

Supplementary Table 1.

Marker genes per cluster.

Supplementary Table 2.

Differentially expressed genes Cluster 2 and 3.

Supplementary Table 3.

Signature gene lists from literature.

All Supplementary Tables are available at DOI: 10.1136/jitc-2025-014041

Supplementary Methods

Vaccination

The Rpl18-Adpgk-Help vaccine was derived from the Help-E7SH plasmid[30] by replacing the E7SH sequence with codon-optimized sequences for mutated Adpgk (cacctggaactcgcgtccatgaccaacatggagctgatgtcctccatcgtgcatcag) and mutated Rpl18 (aaagcaggaggcaagattctgaccttcgacagactggcactgg-agagcccaaaa) epitopes[44], separated by an alanine linker. For both the neoHelp and neoHelp-RA vaccines, the coding sequences of the MC38 tumor-specific helper neoepitopes Pcdh18, Zmiz1, and Ddr2[45] were separated by glycine-proline linkers and preceded by a signal peptide sequence derived from the Help-E7SH vaccine. For the neoHelp-RA vaccine, the helper neoepitopes were linked to codon-optimized sequences for mutated Adpgk and mutated Rpl18, separated by an alanine linker. A 5' 27-base pair and a 3' 26-base pair flanking region with homology to KpnI- and NotI-linearized pVAX1 were added to the neoHelp and neoHelp-RA sequences. The complete DNA sequences were ordered as a gBlock from Integrated DNA Technologies (IDT), and assembled into linearized pVAX1 using NEBuilder HiFi DNA Assembly (New England Biolabs). All vaccines were verified by Sanger sequencing.

Flow cytometry staining

Cells from blood, spleen, LN and tumor were washed with FACS buffer (PBS + 2% FCS) and stained for 30 min on ice with 1:1000 LIVE/DEAD Near IR dye (Invitrogen) or 1:500 Zombie UV (Biolegend), 1:100 APC-conjugated H-2D^b/E7$_{49\text{-}57}$ tetramers, APC-conjugated H-2K^b/OVA$_{257\text{-}264}$ tetramers or APC-conjugated H-2K^b/KILTFDRL (mutated Rpl18) tetramers (produced in-house at LUMC) and combinations of the following monoclonal antibodies (mAbs) for surface staining: 1:100 CD45.1-BUV395 (clone A20, BD Bioscience); 1:100 CD45-BUV496 (clone 30-F11, BD Bioscience); 1:100 KLRG1-BUV563 (clone 2F1, BD Bioscience); 1:100 CD103-BUV661 (clone M290, BD Bioscience); 1:200 CD4-BUV805 (clone GK1.5, BD Bioscience); 1:800 CX3CR1-BV421 (clone SA011F11, Biolegend); 1:200 CD4-BV421 (clone GK1.5, Biolegend); 1:100 SLAMF6-Pacific Blue (clone 330-AJ, Biolegend); 1:100 CD8α-V500 (clone 53-6.7, BD Bioscience); 1:100 CD44-BV570 (clone IM7, Biolegend); 1:50 CXCR3-BV650 (clone CXCR3-173, Biolegend); 1:50 CD127-BV650 (clone A7R34, Biolegend); 1:50 CXCR5-BV711 (clone L138D7, Biolegend); 1:200 CD8α-BV750 (clone 53-6.7, BD Bioscience); 1:100 CD44-BV785 (clone IM7, Biolegend); 1:100 CD39-PE/Dazzle594 (clone Dua59, Biolegend); 1:200 TIM3-PE/Cy7 (clone RMT-23, eBioscience); 1:200 CD43-PE/Cy5 (clone 1B11, Biolegend); 1:100 CD3-PE/Fire700 (clone 17A2, Biolegend); 1:100 CD62L-PE/Fire810 (clone W18021D, Biolegend); 1:200 CD62L-AF561 (clone MEL-14, eBioscience); 1:200 KLRG1-PE/eF610 (clone 2F1, Invitrogen); 1:200 CX3CR1-PerCp/Cy5.5 (clone SA011F11, Biolegend); 1:200 PD-1-PerCP/eF710 (clone J43, eBioscience); 1:100 PD-1-APC/Fire810 (clone 29F.1A12, Biolgend). For intracellular staining, cells were fixed and permeabilized with the FOXP3/transcription factor staining buffer set (eBioscience), according to the manufacturer's protocol. Intracellular staining was performed for 30 min on ice in permeabilization buffer, using combinations of the following mAbs: 1:100 Helios-

BUV395 (clone 22F6, eBioscience); 1:100 TCF-1-AF488 (clone C63D9, Cell Signalling Technology); 1:200 GZMB-PE (clone GB-11, Sanquin); 1:100 TOX-PE (clone TXRX10, eBioscience); 1:100 GZMB-PE/CF594 (clone GB-11, BD Bioscience); 1:100 FOXP3-PE/Cy5 (clone FJK-16s, Invitrogen); 1:800 TOX-eF660 (clone TXRX10, eBioscience); 1:200 T-bet-eF660 (clone eBio4B10, eBioscience); 1:400 T-bet-AF660 (clone eBio4B10, eBioscience); 1:200 Ki67-AF700 (clone SolA15, eBioscience).

scRNAseq analysis

Preparation and quality control - Analysis of scRNAseq and TCRseq data was performed using CellRanger (10X Genomics, v6.0.1) and Seurat (v4.3.0) in R (v4.2.3). scRNAseq reads were aligned to the mouse reference genome mm10, and barcode counting was performed using 'cellranger count'. TCRseq reads were aligned to the mouse reference genome mm10 and consensus TCR sequences were determined using 'cellranger vdj'. From the gene expression count matrix, TCR and BCR genes were removed using the 'grep' function in R with the patterns "^Tr[abgd][cvdj]" and "Ig[hkl][cvdj]" respectively. After this, the dataset was analyzed in R using the standard Seurat pipeline. Seurat object was created using 'CreateSeuratObject', with a minimum of 200 features per cell and 3 cells expressing each gene. HTO sequencing data was added as a separate assay to the Seurat object using 'CreateAssayObject' and HTO counts were normalized by CLR method using 'NormalizeData'. HTO demultiplexing was performed using 'HTODemux' with a positive quantile of 0.99. As a result of this, each cell in the dataset was assigned to a global HTO classification (singlet, doublet, or negative), and a HTO classification (Day-5-Help-dLN, Day-5-Help-ndLN, Day-5-No-Help-dLN, Day 5-No-Help-ndLN, Day-10-Help-dLN, Day-10-Help-ndLN, Day-10-No-Help-dLN, Day 10-No-Help-ndLN, doublet or negative). Heatmap was created of HTO demultiplexing result using 'HTOHeatmap' (Supplementary Figure 6B). Singlets were selected using 'subset', and gene expression data was normalized using 'NormalizeData'. Variable features were determined using 'FindVariableFeaures' with the selection method 'mean.var.plot'. Data was scaled using 'ScaleData' on variable features. Percentage of mitochondrial gene expression per cell was determined using 'PercentageFeatureSet' with the pattern "^mt-". Singlets were filtered on number of RNA features (between 400 and 5000), number of RNA counts (<25000) and mitochondrial gene expression (<10%). Cell cycle scores for G2/M and S phase were assigned using 'CellCycleScoring', based on expression of G2/M and S phase genes. Data was normalized using 'NormalizeData' with normalization method 'LogNormalize', scale factor 25000. Top 2000 variable features were determined using 'FindVariableFeatures' with the selection method 'vst'. Data was scaled using 'ScaleData', whereby G2M scores, S scores and percentage of mitochondrial gene expression were regressed out. Principle component analysis (PCA) was run using 'RunPCA' on variable features. Clustering was performed on first 20 principle components (PCs) using 'FindNeighbors' and 'FindClusters'. Clustering resolution was set to 0.5. Uniform manifold approximation and projection (UMAP) visualization was performed using 'RunUMAP' on the first 20 PCs. Expression of known marker genes was visualized per cluster and within the UMAP projection using 'Dotplot', 'VlnPlot' and 'FeaturePlot' functions. Clusters with contaminating B cells (expression of *Cd19,*

Ms4a1), APCs (expression of *Cd40, Cd274, Cd80, Cd86*) and low quality cells (high percentage mitochondrial genes, low RNA counts) were removed. The pipeline was run again on filtered T cells, including determining variable features, data scaling, PCA, clustering and UMAP visualization. Clustering and UMAP visualization was performed on the first 50 PCs. $CD8^+$ T-cell clusters were selected by expression of *Cd8a, Cd8b1*, in absence of expression of *Cd4* (Supplementary Figure 6C). Within the $CD8^+$ T-cell subset, number of cells per HTO was determined (Supplementary Figure 6D). HTOs containing <30 $CD8^+$ T cells were excluded from further analysis.

Gene expression analysis - The pipeline was run again on $CD8^+$ T cells from selected HTOs, including determining variable features, data scaling, PCA, clustering and UMAP visualization. Clustering and UMAP visualization were performed on the first 20 PCs. UMAP embeddings, cluster annotations and HTO annotations per cell were exported from Seurat, and visualized using Loupe Browser (v6.4.1, 10X Genomics). Marker genes per cluster were calculated using 'FindAllMarkers', selecting only upregulated genes expressed in >25% of cells in the cluster, with a logFC threshold of 0.25. $CD8^+$ T-cell clusters were annotated based on expression of marker genes per cluster, as well as the expression of manually selected genes with well-known functions in T-cell differentiation according to the literature. Functional classification of differentially expressed genes between Cluster 2 and Cluster 3 was performed using Ingenuity Pathway Analysis (Qiagen).

TCRseq analysis - Sequences of CDR3 and VDJ gene annotations of paired TCRα and TCRβ chains were analyzed using Loupe VDJ Browser (v5.0.0, 10X Genomics). Expanded clones were identified as TCR clonotypes containing 2 or more cells. TCR sequences from Loupe VDJ Browser, and UMAP projection and cluster annotation from Seurat were visualized together using Loupe Browser (v6.4.1, 10X Genomics). For determining expanded clonotypes per differentiation cluster, only cells that grouped together in the UMAP with their assigned cluster were included for quantification.

Trajectory analysis was performed using Seurat and Monocle3 (v1.3.1) in R. Seurat object of $CD8^+$ T cells from selected HTOs was converted into cell data set object using 'as.cell_data_set', after which partitions, cluster annotations and UMAP embeddings were added manually. Trajectory was plotted using 'learn_graph', after which the trajectory branch of interest (from Cluster 0 to Cluster 3) was selected using 'choose_graph_segments'. Pseudotime was calculated using 'order_cells', and pseudotime values per cell were exported for visualization using GraphPad Prism and Loupe Browser.

For *comparison of our scRNAseq data to published gene signatures*, top 200 marker genes of $TCF1^+$ progenitor (cluster 9) and effector (cluster 6) $CD8^+$ T cells from chronic and acute LCMV infection were downloaded from Table S5 from Pritykin *et al.* 2021[7]. These top 200 genes were used to calculate a module score for each cell in our $CD8^+$ T cells from selected HTOs, using the function 'AddModuleScore' in R. The same method was performed using top 100 marker genes of stem-like $CD8^+$ T cells from the TdLN, (cluster 4) as published by Connolly *et al.* 2021[41], which were provided upon request.

Generation of MC38-Help cells

pCDH-EF1a-IRES-eGFP was linearized using BamHI-HF and NotI-HF (New England Biolabs, NEB). The HELP coding sequence was fused to a 3xFLAG sequence, and a 5' 20-base pair flanking region (tcaggtgtcgtgagcaattg) and a 3' 20-base pair flanking region (gctacgtaaattccgcccct) were added that are homologous to the linearized pCDH-EF1a-IRES-eGFP. The full DNA sequence was ordered as a gBlock (IDT) and NEBuilder HiFi DNA Assembly (NEB) was used to assemble pCDH-EF1a-HELP-3xFLAG-IRES-eGFP.

Third-generation lentiviruses were produced by transfecting HEK293T cells with pCMV-VSVG, pMDLg-RRE, pRSV-REV, and pCDH-EF1a-HELP-3xFLAG-IRES-eGFP. Medium was refreshed the next day and 48 hours post-transfection lentivirus-containing medium was centrifuged at 700 xg for 10 minutes to remove debris and filtered through a 0.45 µm filter (Millex Low Protein Binding Durapore, Millipore). MC38 cells were reverse transduced with lentivirus encoding EF1a-HELP-3xFLAG-IRES-eGFP in the presence of 8 µg/mL polybrene. Medium was refreshed one day after transduction and eGFP-expressing MC38 cells were sorted one week after transduction to obtain MC38-HELP cells. HELP-3xFLAG expression in MC38-HELP cells was validated by western blot.